UNIVERSITY OF OKLAHOMA

GRADUATE COLLEGE

CHARACTERIZATION OF SURFACTANTS AND TRACER PROPERTIES FOR POTENTIAL EOR APPLICATIONS

A DISSERTATION

SUBMITTED TO THE GRADUATE FACULTY

in partial fulfillment of the requirements for the

Degree of

DOCTOR OF PHILOSOPHY

By

SHENGBO WANG
Norman, Oklahoma
2017

CHARACTERIZATION OF SURFACTANTS AND TRACER PROPERTIES FOR POTENTIAL EOR APPLICATIONS

A DISSERTATION APPROVED FOR THE
MEWBOURNE SCHOOL OF PETROLEUM AND GEOLOGICAL ENGINEERING

BY

_____
Dr. Bor-Jier Shiau, Chair

_____
Dr. Jeffrey H. Harwell

_____
Dr. Ahmad Jamili

_____
Dr. Xingru Wu

_____
Dr. Maysam Pournik

To my families

Acknowledgements

I would like to express my deepest gratitude to my advisors Dr. Bor-Jier Shiau and Dr. Jeffrey H. Harwell for their guidance and advice throughout my Ph.D study. I thank them for the consistent encouragement and patience they showed to me during all these years. Without their support, I would not have been able to accomplish this study today.

I would also like to thank ASL (Applied Surfactant Laboratories), CFT (Chemical Flood Technology) and AEC (Advanced Energy Consortium) for their funding.

I would also like to express my thanks to all my committee members: Dr. Bor-Jier Shiau, Dr. Jeffrey Harwell, Dr. Ahmad Jamili, Dr. Xingru Wu and Dr. Maysam Pournik.

I would like to express my warm thanks to all my friends at OU not only for friendship but also for scientific discussions and advice from Changlong Chen, Zahra Shahrashoob, Shuoshi Wang, Wei Tian, Hao Li, Sangho Bang.

Last but not least, I would like to thank my parents and my family for their unconditional love and encouragement.

Table of Contents

List of Tables

List of Figures

Abstract

There are some challenges in chemical flooding, such as, gas finger problem usually occurred in field tests, potential scale problems of chemical slug caused by precipitation due to incompatibility between chemical solution and formation brine, and drawbacks of experimental designing of chemical flooding. In this work, three challenges are mainly discussed in following chapters. Chapter one focuses on optimization of designing single well test; chapter two discusses the feasibility of foam stabilized by nanoparticles in porous media; chapter three states that coacervates problems are occurred in preparation of chemical solutions. The summary of three topics is addressed below.

The first chapter, the single well chemical tracer test (SWCTT) has emerged in the past decades as a method for measuring oil saturation prior to and/or after EOR operations, to measure the recovery performance *in-situ*. To use this technology, the partition coefficients of the selected tracers are essential for estimating the level of residual oil at the targeted single well. Commonly, injection of short chain alcohols and ethyl acetate, a reactive tracer, is carried out for the tracer slug, mainly based on site-specific reservoir conditions, to accurately determine the level of oil saturation in-situ. However, injection of ethyl formate has been less common due to its fast hydrolysis rate under elevated temperature, which increases the challenges in data interpretation. Therefore, a systematic study for using ethyl formate under mid-range temperature (<60 ℃); -as commonly found in mature oil field in the U.S., show the potential to be applied for SWCTT.

As part of the design effort for a series of EOR field tests to manage the project risk, we particularly assessed the relationships between the partition coefficients of reactive tracers and subsurface conditions; -such as salinity, temperatures, type of electrolytes and the equivalent alkane carbon number (EACN) of the crude oil experiments were performed under various reservoir conditions as a function of actual site characteristics at the targeted high saline formations.

In brief, our data clearly show that the (oil/water) partition coefficient of ethyl formate increase steadily with increasing NaCl concentrations, ranging from 10,000mg/L (0.17M) to 250,000mg/L (4.28M). A similar upward trend was observed for increasing temperature between 25℃ to 52℃; however, the partition coefficient decrease inversely with increasing the crude oil EACN over the range from 8 to 12, which are common for domestic oil samples. It was also showed that brine with high NaCl concentration yielded higher partition coefficients. In contrast, brine with high $CaCl_2$ and $BaCl_2$ concentration yielded lower values. And $MgCl_2$ performed somewhat unusual trend in our tests. These results further indicate that the partition coefficient of the reactive tracer, ethyl formate, is sensitive to change in salinity, temperatures, type of electrolytes and EACN, as observed for other chemical tracers. In addition, based on the hydrolysis rate of ethyl formate under various reservoir conditions, the appropriate window of shut-in time can be pre-determined before initiating the field test. We believe that the ability of better understanding the partition coefficients and predicting the shut-in time beforehand could drastically reduce the risks of SWCTT operations.

In second chapter, the application of nanoparticles dispersions in foam flooding has become an attractive chemical enhanced oil recovery (EOR) technique as compared to

conventional surfactant only foaming system. This study is to expand our understanding of utilizing multi walled carbon nanotube (MWCNT) on foam stability in porous media. We developed several foaming agent formulations (surfactants and polymers) in the presence of MWNT in 3% salinity (NaCl, 2.4wt%, $CaCl_2$, 0.6wt %). The dispersion stability of the MWCNT and the viscosity of the solutions were measured. Foam was generated *in-situ*, one-dimensional flow-through tests were performed by co-injecting air and foaming solution containing either the foaming agents-only or the foaming agents in the presence of MWCNT. During each experiment, the pressure drop (Δp) and the nanoparticles recovered across the sand-pack were monitored. Injection rate, gas fraction and the effect of MWCNT stabilized foams in porous media were investigated.

The results reveal that foams stabilized by nanoparticles are able to generate stronger foams leading to apparent higher Δp by introducing MWCNT that total concentration is as low as 60ppm. Δp profile varies with gas fraction which largely affects the foam texture. Also, our data indicate the viscosity of foaming agent solutions influences Δp values. Adding MWNT to the foaming agent solutions appears beneficial to the flooding as surfactants adsorb to nanoparticles which facilitates surfactants partitioning to the G/L interface.

Thus, addition of nanoparticles in the developed surfactant-polymer foam formulations can lead to formation of stronger high-quality foams in porous media, which improves the sweep efficiency and increases the oil recovery.

In third chapter, large amounts of surfactant coacervation work were focused on complex coacervation, such as mixture of surfactant and polymer, or mixture of different species of surfactants, seldom on the simple coacervation of single

conventional surfactant in aqueous phase. This study aims to investigate evolution of dioctyl sulfosuccinate (AOT) /sodium chloride coavervation in aqueous solution associated with change in counterion binding degree.

In this work, coacervation phase boundary of AOT in the presence of sodium chloride was obtained by spectrophotometer in terms of turbidity measurement. The activity of counterion was measured by sodium ion electrode probe. Electro kinetic parameters such as hydrodynamic aggregate size were investigated by dynamic lighting scattering (DLS).

A monotonic decreasing AOT coacervate boundary was observed with increase in NaCl concentration. The degree of counterion binding, calculated by modified Corrin-Harkins equations, revealed a 3-segment behavior of AOT in salt solution. Colloid size distribution was conducted with DLS.

Counterion binding degree plays an important role in the formation of surfactant aggregates. A further study of binding degree facilitates to understand coacervation.

Chapter 1. Effect of Reservoirs Conditions on Designing Single-Well Chemical Tracer Tests under Extreme Brine Conditions

1.1 Introduction

Chemical tracer is a powerful technology for reservoir characterization (Tian, 2016). Accurate estimate of residual oil saturation is a crucial step for many aspects of reservoir characterization and even more important in the economic attractiveness of a planned water flooding or a proposed tertiary recovery operation. The SWCTT, a proven effective and feasible methodology has been widely used for measuring oil saturation in-situ before and after the application of enhanced oil recovery operations, such as chemical flooding (Huseby and Sagen, 2012). The SWCTT is a rapid process for measuring residual oil saturation, commonly last 3 to 5 days per test, via the injection and then reverse production of brine carrying a suite of chemical tracers targeting at a near-well region of 15 to 20 feet from the wellbore (Tomich and Dalton 1973). During the tracer test, the reactive (primary) tracer, usually a short chain ester (e.g., C_3 to C_5), is dissolved in formation brine and injected into a production well. The slug of tracer bank is pushed away from the wellbore through injecting finite volume of tracer-free formation brine traveling to pre-determined distance (15 to 20 ft). Following the injection, the tested well is then shut in temporary (typically 36 to 48 hous) to allow the primary tracer to be hydrolyzed with the reservoir brine in order to produce the secondary tracer, a short-chain alcohol, while portion of total ester injected also partitioning into crude oil if present. After shut-in time lapsed, the production of the studied well is resumed and the concentration profiles of the primary tracer and the secondary tracer are simultaneously measured in the collected effluent samples (Deans

and Carlisle 2007). The methodology of tracer test offers exceptional advantage of obtaining rather representative measure of residual oil in-situ as better alternative or complement to well logging and core analysis, two other petrophysics methods for determining oil saturations. In last decade, the SWCTT has been commonly carried out to evaluate the performance and effectiveness of EOR effort.

The early SWCTT test was reported at an East Texas Field in 1968 by Exxon Production Research Co. (Deans and Carlisle 1986). Since it was invented, more than few hundreds of SWCTTs have been carried out in a wide range of conditions and formations (Deans and Carlisle 2007). A large amount of literature about SWCTT mostly for measuring residual oil saturation can be found. Among these, Tomich and his colleagues first provided detailed description of the SWCTT method and presented the framework of mathematical model of the process (Tomich et al., 1973), alongside with several U.S. patents (U.S. Patents No. 3,590,923 (1971), No. 3623842 (1971)). Bragg et al. presented field data of SWCTT and studied the test sensitivity to the measured residual oil saturation. They also gave two examples to illustrate how the residual oil saturations measured in these tests have been combined with other reservoir data to better evaluate water flood conformance (Bragg and Carlson, 1976). Mechergui and coworkers proposed a modified approach of a designing of SWCTT specifically for high temperature and high salinity conditions using the numerical simulation tool for proper screening the right tracers. Their conclusions highlighted the importance of the partitioning coefficient (K_d) and hydrolysis reaction rate (K_h) in SWCTT and suggested the criteria of tracer selection (Mechergui et al., 2012). A significant portion of these published work have focused on the preparation and operation of field tests,

interpretation of the field data and simulation work of SWCTT tests. Based on these prior efforts, it is quite obvious that most crucial questions to be addressed for planning a SWCTT are the proper selection of primary reactive tracers and the pre-determined of shut-in time enabling to generate adequate secondary tracer as a result of the hydrolysis reaction. Thus, the success of a tracer test is governed by accurate determining the partitioning coefficient, K, a key parameter in SWCTT (Majluf et al., 2012). The SWCTT theory calls for well-defined chromatographic retardation of a tracer chemical that is soluble both in formation brine and in crude, while the oil is basically stationary and the formation brine is steadily moving. The hydrolysis reaction of the ester tracer injected will ideally lead to the production of alcohol and acid stoichiometrically. Since the partitioning coefficient of the product alcohol between oil and brine is basically approaching zero, thus the produced alcohol is dissolved only in brine and absence in the oil phase. When the tested well is resumed its production during the pull-back, the product alcohol distinctly separates from the un-reacted ester tracer if significant amount of oil is still present in the targeted zone. In general, the product alcohol travels at a higher velocity than the ester tracer in the water, causing the alcohol to return to the well earlier than does the un-reacted ester tracer. This phenomenon is known as chromatographic retardation.

The equilibrated distribution of the partitioning tracer between different crude and brine phases is governed by the value of partitioning coefficient. And the actual partitioning coefficients were largely affected by three of the site-specific parameters: reservoir temperature, formation brine salinity and oil hydrophobicity, EACN. Thus, these site-related parameters dominantly control the outcome of the hydrolysis reactions that take

place during shut-in period of the tracer test. It is of great value to accurately estimate how these factors affect the partition coefficient and rate constant, which are the key parameters for screening the proper tracer candidates and finalizing the design of shut-in time for a successful field test. Most SWCTTs involved co-injection of a suit of short chain alcohols (conservative) and esters (commonly, ethyl acetate, or propyl formate - the reactive tracer), composing the chemical slug. Not surprisingly, use of ethyl formate appeared less common due to its much rapid hydrolysis rate under elevated reservoir temperature, which inevitably increases the uncertainty of sample analyses and data interpretation as residual ester level quickly approaching the detection limit of analytical instrument. Therefore, there is a need of generating additional data set for ethyl formate, in particular among mid temperature range (<60 ℃) and elevated electrolyte levels (>130,000 mg/L total dissolved solids (TDS)); -as commonly found at mature oil field in mid-continental United States, for its potential for field SWCTT.

1.2 Experiments

1.2.1 Materials

The Ethyl Formate (EF, C_2H_5OOCH) and Ethanol (EtOH, C_2H_5OH), and Methanol (MeOH, CH_3OH) were obtained from Sigma-AldRich, with purities of 97%, 99.5% and 99%, respectively. Three types of representative oil, octane (C_8H_{18}, 99%), decane ($C_{10}H_{22}$ 99%), dodecane ($C_{12}H_{26}$, 99%), and different electrolytes, sodium chloride (NaCl 99%), calcium chloride ($CaCl_2$ 99%), magnesium chloride ($MgCl_2$, 99%) and barium chloride ($BaCl_2$ 99%) were also purchased from Sigma-AldRich. The crude oil was collected at an oil field located in northwestern Oklahoma near Guymon. The

deionized water (DI) was used in all studies for dilution. All chemicals were used as received.

1.2.2 Methods

1.2.2.1 Effect of different electrolytes and salinity on the partition coefficient

Most of the partitioning tests were conducted using ethyl formate, methanol, decane, sodium chloride, calcium chloride, magnesium chloride and barium chloride, unless described elsewhere. The stock solutions for individual electrolyte tested were prepared by dissolving the salt with DI to a concentration of 250,000 mg/L. With the original stock solutions, a set of five different electrolyte concentrations were prepared for each group tests: 10,000 mg/L, 50,000mg/L, 75,000mg/L, 100,000mg/L, and 150,000mg/L. The equal amount of ethyl formate was introduced in individual vials to achieve 5000 mg/L (0.068M) tracer level. Lastly, equal volumes of oil and aqueous phase, (3mL (decane) versus 3mL (5,000mg/L (0.068M) ethyl formate/salt solution), were mixed to five (10mL) glass reactors to assess the kinetics of hydrolysis reaction at different reaction periods: 20, 40, 60, 90 and 120 minutes. Initially, all reactors were shook with a vortex mixer (Vortex Jr. Mixer) for five minutes and left for equilibration at 25℃. Once the reaction time lapsed, individual vial was removed and place in a centrifuge for five minutes at 2000rpm. This facilitates a complete separation between the aqueous solution and non-aqueous liquid phase (decane). Finally, 50μL aqueous sample was withdrew and run on the gas chromatographer equipped with an auto-injector to quantify the concentrations of ethyl formate and ethanol. Unless specified elsewhere, most kinetics studies were conducted at 25 ℃, room temperature.

1.2.2.2 Effect of temperature and EACN on the partition coefficient

A series of solutions, each with different NaCl concentrations of 20,000mg/L (0.34M), 100,000mg/L (1.71M), 170,000mg/L (2.9M) and 250,000mg/L (4.28M), were prepared in a 100-mL volumetric flasks. In addition, each flask contains both 10,000mg/L (0.135M) of ethyl formate and 10,000mg/L (0.312M) of methanol (a mass balance tracer). It is critical to ensure that the ethyl formate has completely dissolved into the brine solutions. Then, the dissolved ethyl formate was introduced (12 mL per vial) into a 24 mL-glass vial. After that, equal volume of oil (12 mL) was also added to individual glass vial with minimum headspace. Three types of oil (non-aqueous liquid) were tested under four types of salt levels. A total of twelve reactors were prepared to quantify the partitioning coefficient over different reaction periods: 30, 60, 90 and 120 minutes. We assessed the temperature effects on tracer partitioning coefficient over three temperature ranges: 25 ℃, 40 ℃ and 52 ℃.

1.2.2.3 The hydrolysis test in crude oil

In addition to the pure oil and the synthetic salt solutions, similar hydrolysis study was conducted using the crude and brine samples retrieved from the target single-well test site located in Guyman, Oklahoma. All reactors were maintained in a 52 ℃ oven to imitate site-specific reservoir temperature. The pre-determined sampling times lasted 48 hours since the shut-in time of field test was what the study concerned. After hand-shaking and leaving all the reactors prepared in the oven (52 ℃), all samples withdrawn from the aqueous phase were run on the gas chromatographer, Agilent GC 5890, equipped with the FID detector to monitor the ethyl formate and ethanol concentrations.

1.3 Theory

The theory of SWCTT is based on the injection of an ester tracer into the reservoir. Some of the injected ester hydrolyzes during shut-in time, and subsequent recovery of the residual ester and the alcohol produced in the producing well yield distinct tracer production profiles that can be further analyzed to measure the oil saturation in-situ at the targeted area. From literature reviews, the most common ester utilized and studied in SWCTT was normally ethyl acetate. However, the ester used in this work is ethyl formate. The selection of proper reactive tracer is largely controlled by reservoir temperature. The ethyl formate is more suitable in the lower reservoir temperatures ranging from 22 ℃ to 58 ℃ and its hydrolysis rate is about 50 times faster than the ethyl acetate at similar temperature. Thus the slower reacting ethyl acetate is normally used in the elevated reservoir regions between 55 ℃ and 122 ℃ (Deans and Carlisle 2007).

For ethyl formate, the hydrolysis reactions can be expressed by Eqn. 1.1,

$$CH_3COOCH_3 + H_2O \rightleftharpoons CH_3CH_2OH + HCOOH \qquad (1.1)$$

The solubility preference of ethyl formate is represented by the oil/water partitioning coefficient, K, where

$$K = \left(\frac{C_{oil}}{C_{water}}\right)_{at\ equilibrium} \qquad (1.2)$$

C_{oil}: Concentration of ethyl formate in oil (M, or mg/L)

C_{water}: Concentration of ethyl formate in water (M, or mg/L)

When equal volumes of the non-aqueous liquid and aqueous solution were added to a vial, and equilibrated, Eqn. (1.2) is used to determine the partitioning coefficient. When the volume ratio of the non-aqueous liquid to aqueous solution is different, the modified

Eqn. (1.3) should be used instead to calculate partitioning coefficient to compensate the effect of unequal ratio of O/W.

$$K = \left(\frac{C_{oil}}{C_{water}} \cdot \frac{V_w}{V_O}\right)_{at\ equilibrium} \quad (1.3)$$

where

V_w: Volume of aqueous solution added to the vial

V_O: Volume of non-aqueous liquid added to the same vial

From Eqn. (1.2) and Eqn. (1.3), it has been demonstrated that partitioning coefficient is not affected by different ratios of the non-aqueous liquid to the aqueous liquid added to a vial.

1.4 Results and Discussion

1.4.1 Effect of electrolytes on the partition coefficient

The effect of four electrolytes on the partition coefficient of ethyl formate and decane was analyzed. The results are presented in Fig.1.1. The results for $BaCl_2$, $CaCl_2$ and $MgCl_2$ were adopted from Chavez's work (Chavez, 2012).

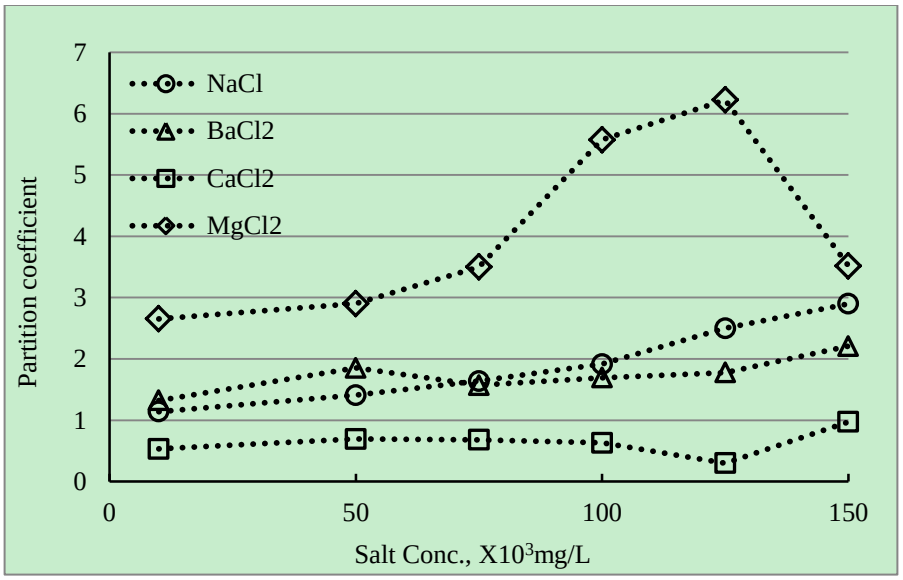

Figure 1.1-1 Partition coefficient of 5,000 mg/L ethyl formate in decane/water with various electrolytes and different concentration at 25 ℃

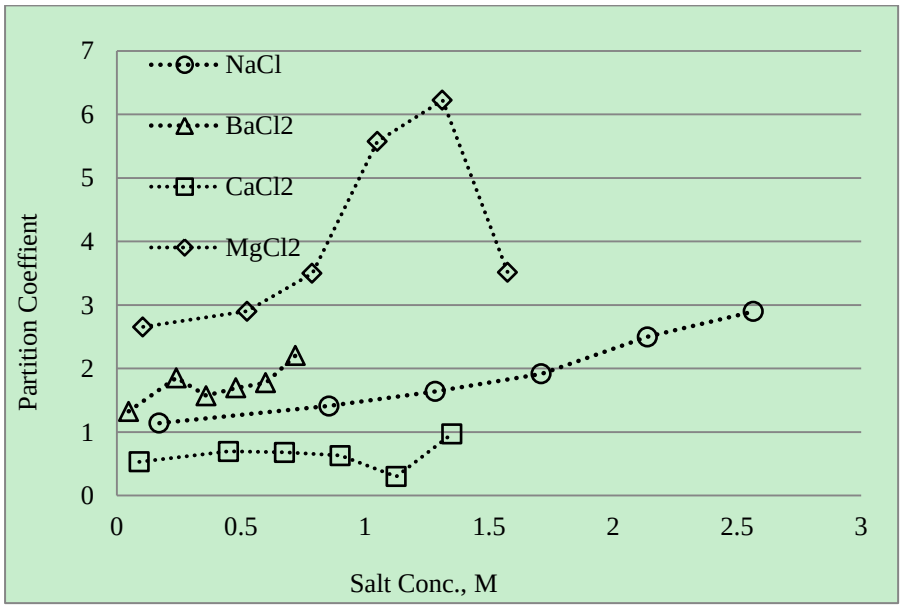

Figure 1.1-2 Use molar concentrations to depict the partition coefficient of 0.068M (5000mg/L) ethyl formate in the same conditions as that presented in Fig.1-1

As shown in Fig. 1.1-1 and Fig. 1.1-2, the partition coefficients in three different electrolytes (NaCl, $BaCl_2$, and CaCl2) are a growing tendency with the electrolytes concentration increasing. $MgCl_2$ exhibited different trend as compared to the rest of the electrolytes. The partition coefficient affected by NaCl and $BaCl_2$ are more prominent

than that of $CaCl_2$. It is important to highlight that the chemical composition of reservoir brines may contain more than the chosen electrolytes that are investigated in this study. The aim of this work is designed to investigate the effect of neutral salts individually. Some reservoirs may contain high quantities of the salts investigated in this work; other reservoir brines may not contain some of these salts whatsoever.

Ca^{2+} has a small ionic radius; therefore it has a high charge density. It can be resolved that the ethyl formate is salting out and its solubility in the aqueous phase decreases. The details of the salting out of ethyl formate will address in the following part.

Addition of $MgCl_2$ up to 150,000mg/L (1.58M) in the aqueous phase has significant effects on the partitioning coefficient. As the concentration of $MgCl_2$ increased to 125,000mg/L (1.31M), the values of partitioning coefficient present an increase tendency. Thus, it is more hydrophobic below 125,000mg/L (1.31M) in comparison to NaCl, $BaCl_2$ and $CaCl_2$. Once the solution reaches $MgCl_2$ concentration of 150,000mg/L (1.58M), the partitioning coefficient drastically drops, thus, indicating that the ethyl formate becomes more soluble in the aqueous solution.

According to Burgess, (1978, 1988), Mg^{2+} has a hydration number of 6; thus, it has the ability to attract and associate six molecules of water around its first hydration shell, shown in Figure. 1.2. For Mg^{2+}, water molecules will arrange themselves with the oxygen ion oriented towards the Mg^{2+} ion, with the hydrogen ions exposed in the outer layer of the gathering.

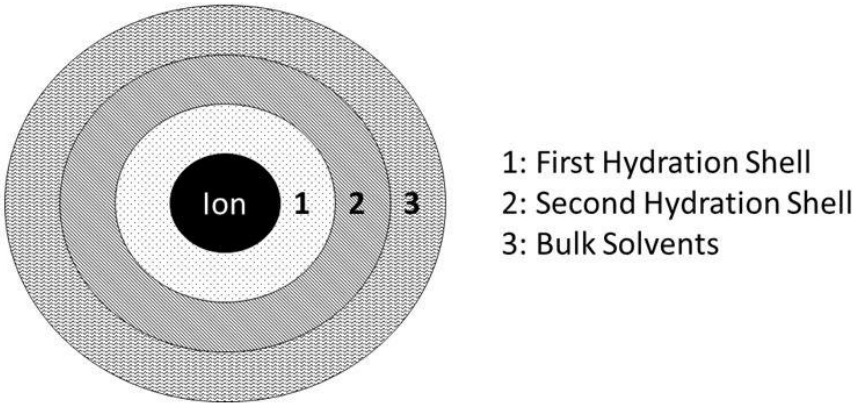

Figure 1.2 The environment of an ion in aqueous solution (Adopted from Burges 1988)

Increase in the concentration of $MgCl_2$ in the system leads to a higher attraction of water molecules around the Mg^{2+} ion due to its strong electronegativity, 1.31 (Shannon, 1976), consequently, weakening the water-water interaction. Therefore, as the concentration of $MgCl_2$ reaches a level of 150,000mg/L (1.58M) in the aqueous solution, the increment on the aggregation of hydrated Mg^{2+} clusters lead to an increase on the solubility of ethyl formate in the aqueous solution.

Mg^{2+} has a higher electronegativity value than that of Ca^{2+} and Na^{+}, (1.31, 1.0, 0.93 respectively, (Shannon, 1976), therefore, water molecules are highly attracted to Mg^{2+} ion in comparison to the Ca^{2+} and Na^{+} ions. This leads to a faster formation of hydrated Mg^{2+} clusters at lower concentration in comparison to the Ca^{2+} and Na^{+} systems.

By closely assessing Figure 1.1, it is observed that at a Mg^{2+} concentration of 150,000mg/L (1.58M) the partitioning coefficient significantly drops, thus the aqueous solution shifts from an ethyl formate insolvable to an ethyl formate soluble system. This can be attributed to a high concentration of Mg^{2+} hydrated clusters leading to predominance of the hydrated phenomenon over the salting-out phenomenon in the aqueous phase, shown in Figure. 1.3.

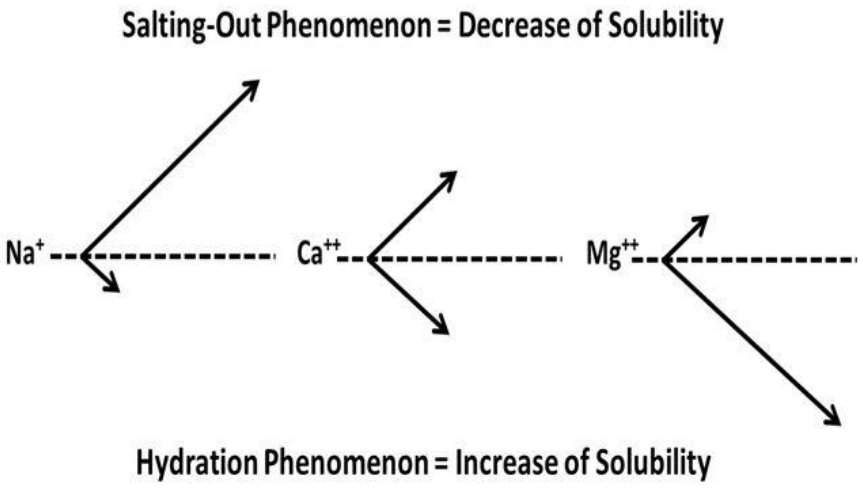

Figure 1.3 Preference of different neutral salts over the salting-out phenomenon versus the hydration phenomenon (Adopted from Chavez, 2012)

1.4.2 Effect of salinity on the partition coefficient

In Fig. 1.4 – 1.6, the partition coefficients are measured in presence of NaCl-only with three types of oil, decane, dodecane and octane system, respectively. As seen in these figures, the partition coefficients increase with increasing salt (NaCl) concentration no matter at what temperature. This phenomenon results from the bulk of ethyl formate molecules dissolved in water were driven to the non-aqueous liquid zone because of decreasing solubility with the increase of salinity in aqueous phase.

Ethyl formate is a short-chain ester with a molecular weight of 74.08 g/mole. It is fairly soluble in both water and non-aqueous liquid. However, solubility-in-water deceases as the length of hydrocarbon chain of ester increases. In other words, the larger the ester molecule is, the less soluble in water it is. The reason responsible for the ester solubility is that it is capable of forming the hydrogen bonds with water molecules. Part of the slightly positively-charged hydrogen atoms in a water molecule can provide sufficiently attraction to one of the ion-pairs on oxygen atoms of ethyl formate for the hydrogen bond to be formed. When salt is added into a mixture of immiscible solvents, there is an

increase of high ionic strength in aqueous environment. According to Chen and Adelman (1980), ions with smaller ionic radius carry a higher charge density. Na^+ has an ionic radius of 102 pm (Shannon, 1976); therefore it has a high charge density. According to Zangi and Berne (2006), ions with high charge density increase the propensity of the hydrophobic molecules to aggregate. This corresponds to stronger hydrophobic interactions between the organic molecules (ethyl formate) due to the increase of the ionic strength in the aqueous phase. Some of the water molecules are now attracted by the salt ions, which decreases the number of water molecules available to interact with the carboxyl group of ethyl formate. As a result of the increased demand for water molecules, the interactions between the ethyl formate and non-aqueous liquid layer are stronger than the ethyl formate-water interactions. The ethyl formate molecules gradually move to the non-aqueous liquid regime, thereby decreasing its solubility in aqueous phase, other known as the salting-out phenomenon. This process results in an increase of the concentration of ethyl formate in the organic phase and a decrease of ethyl formate concentration in aqueous phase. Ultimately, it leads to the increase of partitioning coefficient of ester.

1.4.3 Effect of temperature on the partition coefficient

In addition to the relationship between partition coefficient and salinity was shown in Fig. 1.4 – 1.6, these curves also depict the effects of temperature on the partition coefficient. The experiments were conducted at three different temperatures 25 ℃, 40 ℃, 52 ℃. Increasing temperature results in a general upward trend of increasing the partitioning coefficient.

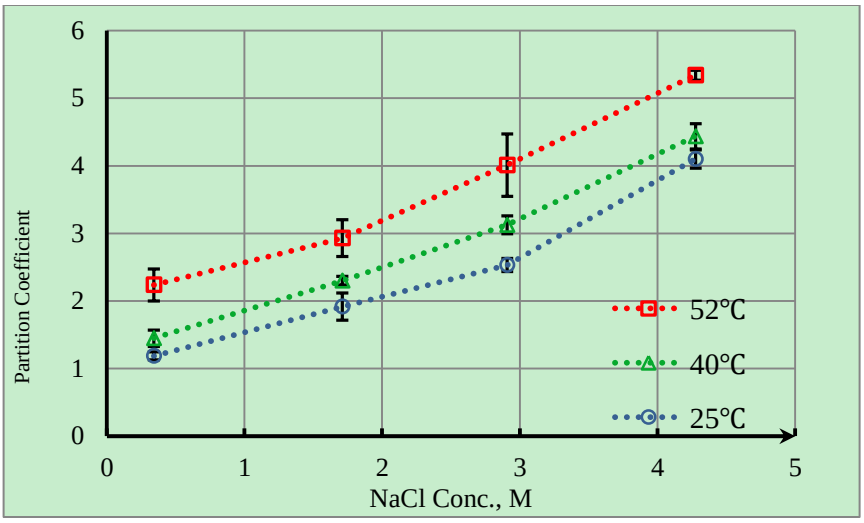

Figure 1.4 Effect of temperature and salinity on partition coefficient in water/decane solvent

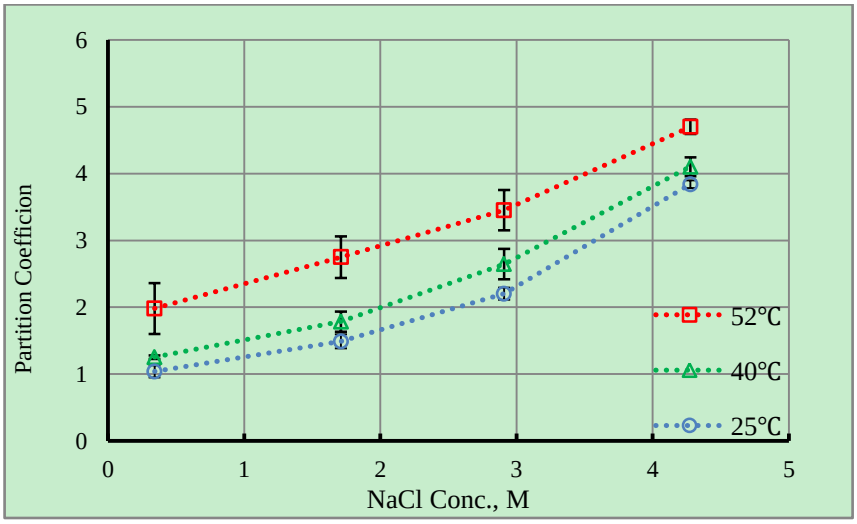

Figure 1.5 Effect of temperature and salinity on partition coefficient in water/dodecane solvent

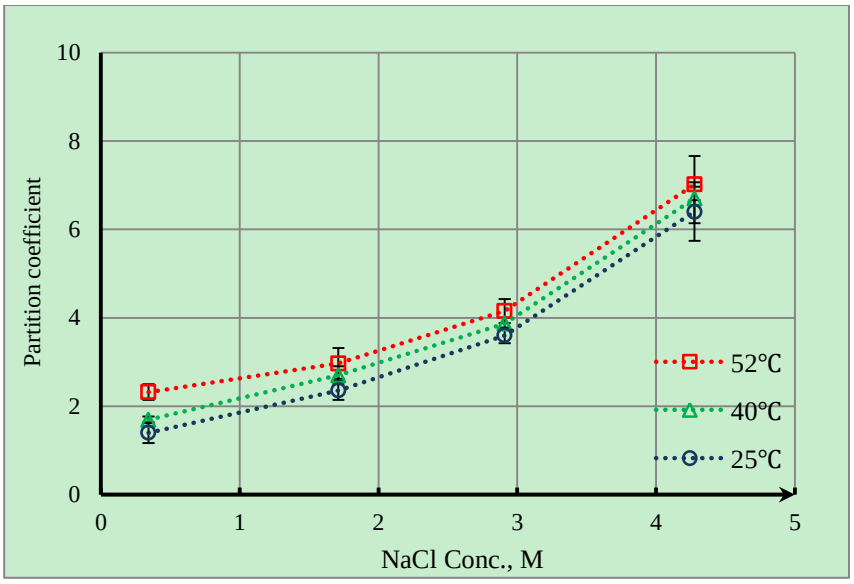

Figure 1.6 Effect of temperature and salinity on partition coefficient in water/octane solvent

Thus, reservoir temperature would be one of the key designing parameters affecting the partition coefficient. The positive correlation between increase of temperature and the growth of the partition coefficient is obvious, especially for the cases of C_{10} and C_{12} alkanes (Fig. 1.4 – 1.6). One plausible explanation is that esters are easily cleaved to carboxylic acids and alcohols in the presence of excessive weak acid under aqueous condition. The hydrolysis of ester requires additional thermal energy proceed at a reasonable rate because it involves an endothermic process (Vollhardt, 2009). Increasing reaction temperature results in even greater number of ester molecules in water participating in the hydrolysis. To maintain the concentration gradient of ester distributed in both the aqueous and non-aqueous phases, additional ester molecules in oil phase have to migrate to compensate the depleted-aqueous phase concentration. Thus, the partitioning coefficients become larger at high temperature. The other plausible explanation is that the water molecules move around faster and collide with the particle with more force that makes the particle move more quickly at higher

temperatures because of Brownian motion. As a result of increased motion of the water molecules, the hydrogen bond between the water molecule and ethyl formate molecule is less likely to form.

1.4.4 Effect of EACN on the partition coefficient

For constant temperatures and salinities, the partition coefficient is measured in NaCl with three different non-aqueous phase liquids (C_8, C_{10}, C_{12} alkanes). The resulting partitioning coefficients and the corresponding standard deviations at three temperatures conditions are summarized in Tables.1.1- 1.3.

Table 1.1 Effect of EACN on partition coefficient at 25 ℃

	NaCl: 20,000mg/L		NaCl: 100,000mg/L		NaCl: 170,000mg/L		NaCl: 250,000mg/L	
EACN	K	SD	K	SD	K	SD	K	SD
8(octane)	1.6	0.2	2.4	0.2	3.7	0.2	6.6	0.23
10(decane)	1.2	0.1	1.9	0.2	2.5	0.1	4.1	0.1
12(dodecane)	1	0.1	1.5	0.1	2.2	0.1	3.8	0.1

*K: partition coefficient
* SD: standard deviation

Table 1.2 Effect of EACN on partition coefficient at 40 ℃

	NaCl: 20,000mg/L		NaCl: 100,000mg/L		NaCl: 170,000mg/L		NaCl: 250,000mg/L	
EACN	K	SD	K	SD	K	SD	K	SD
8(octane)	1.7	0.1	2.7	0.2	3.9	0.1	6.7	0.9
10(decane)	1.5	0.1	2.3	0.1	3.1	0.1	4.4	0.2
12(dodecane)	1.2	0.02	1.8	0.2	2.6	0.2	4.1	0.1

Table 1.3 Effect of EACN on partition coefficient at 52 ℃ (reservoir temperature of War Party)

	NaCl: 20,000mg/L		NaCl: 100,000mg/L		NaCl: 170,000mg/L		NaCl: 250,000mg/L	
EACN	K	SD	K	SD	K	SD	K	SD
8(octane)	2.3	0.2	3	0.3	4.2	0.27	7	0.1
10(decane)	2.5	0.2	2.9	0.3	4	0.463	5.3	0.1

12(dodecane)	2	0.4	2.8	0.3	3.5	0.303	4.7	0.1

As seen in above three tables, with an increase in EACN, the tendency of partition coefficient is a general reduction on the basis of the constant salinities and temperatures. This is consistent with previous research by Thal and Knox (2007) in which they found that partition coefficients of short-chain alcohols increased with decreasing n-alkane carbon number. Dwarakanath and Pope (1998) also reported similar relationship between tracer partition coefficients and the EACN of oil. The decrease of in partition coefficients is likely due to the decreased entropy of mixing (Wu and Sabatini, 2000).

1.4.5 Determination of shut-in time

Results of the hydrolysis rate data of ethyl formates and the produced alcohols at two temperatures (40 ℃, 52 ℃) are depicted in Figs. 1.7 and 1.8. Initial ethyl formates concentration in stock solution is kept at constant 10000mg/L (0.135M). In these set of tests, the salinities and non-aqueous liquid phase used in the two tests are 100000mg/L (1.71M) NaCl and decane ($C_{10}H_{22}$), respectively. The initial test was conducted over 30 min-periods for producing enough alcohols that can be detected by gas chromatographer. As seen in Fig. 1.7, the experiment was ceased at 26 hours because the concentration of alcohols and ethyl formates in the aqueous phase reached exceedingly low levels (below the detection limit of GC used), making it impossible for detecting any further change between 26 to 48 hours.

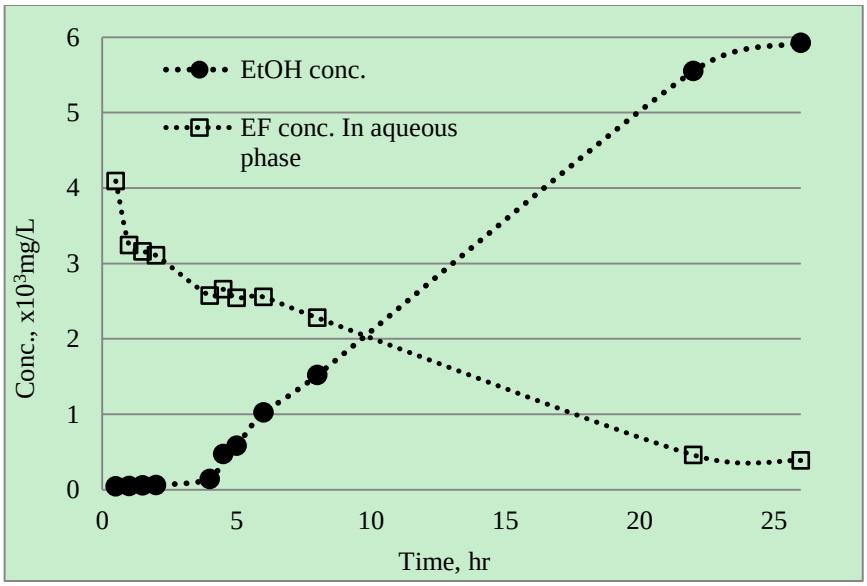

Figure 1.7 Hydrolysis of 10000mg/L ethyl formats in water/decane mixture at 40 ℃

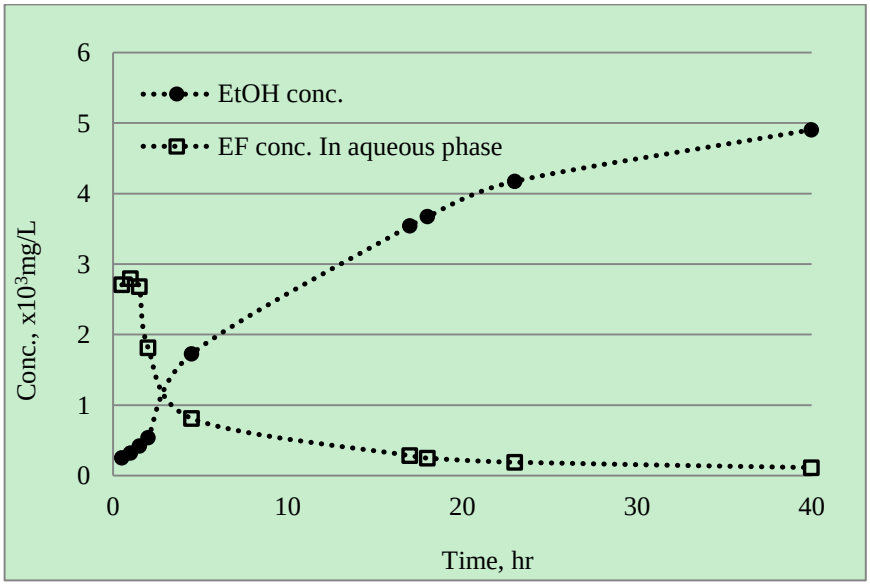

Figure 1.8 Hydrolysis of 10000mg/L ethyl formats in water/decane mixture at 52 ℃

The ideal shut-in period must be long enough for this hydrolysis reaction to proceed to anywhere from 10% to 50% completion (Deans and Carlisle 2007). Based on this criterion and through interpolation method, we expect that the reasonable shut-in time for ethyl formate ranges from 5.25 hours to 14.76 hours at 40 ℃, and ranging from 2.32

hours to 17 hours at 52 ℃. Assuming pseudo-first order rate, the estimate reaction rate constant are 0.0513/hr at 40 ℃ and 0.3296/hr at 52 ℃. This difference is caused by temperature effects.

The hydrolysis data of ethyl formates for designing a field pilot SWCTT test are shown in Fig. 1.9. The crude oil and brine was retrieved from an oil field located in Guyman, Oklahoma with a reservoir temperature of 52 ℃. The brine TDS salinity is 26%.

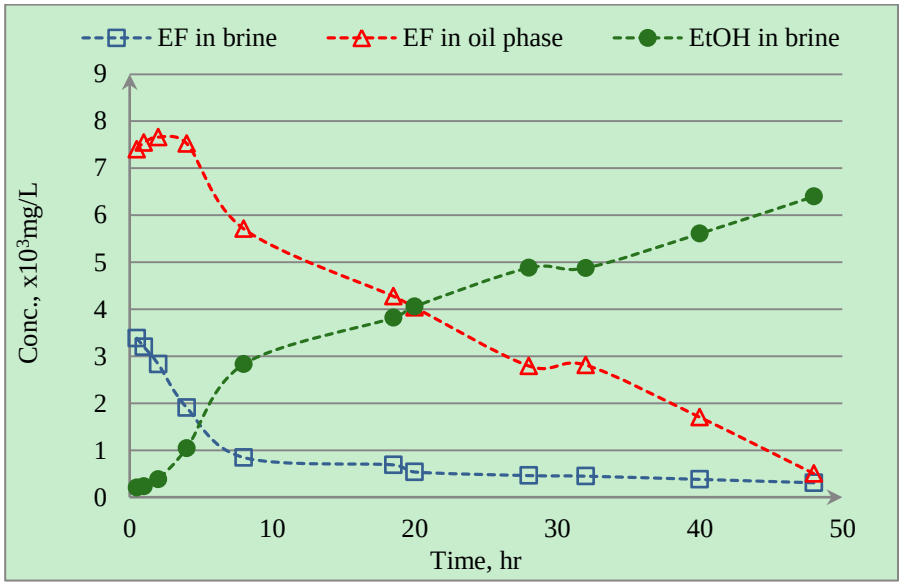

Figure 1.9 Hydrolysis of 10000mg/L ethyl formats in brine/crude oil solvent at 52 ℃

As seen in Fig. 9, the values of ethyl formate in oil phase are the calculated data results based on mass conservation of ethyl formate added initially and ethanol produced. Both the values of ethyl formate in oil phase and in aqueous phase decrease along with reaction time. However, the measured ethanol concentrations in aqueous phase increase over the reaction period. These trends basically match with the predicted values based on the kinetics study and the mass conservation theory. Based on the criterion presented by Dean and Carlisle, it is reasonable to assume that the shut-in time of the pilot test at war party site should be around 4 hours to 14.7 hours.

1.5 Conclusions

This research discussed that several key parameters affect the partition coefficient of ethyl formates tracer prepared for designing, a field pilot SWCTT under extreme high TDS conditions. Our observations clearly show that the (oil/water) partition coefficient of ethyl formate increase steadily with increasing NaCl concentrations, ranging from 10,000mg/L (0.17M) to 250,000mg/L (4.28M). A similar trend was observed for increasing reservoir temperatures between 25℃ to 52℃; however, the partition coefficient decrease inversely with increasing the crude oil EACN values over the range from 8 to 12, which are commonly found for U.S. domestic crude. It was also showed that brine samples with high NaCl concentration yielded higher partition coefficients. In contrast, brine with high elevated $CaCl_2$ and $BaCl_2$ concentrations typically yielded lower values. And $MgCl_2$ performed somewhat unusual trend in our tests. These results further indicate that the partition coefficient of the reactive tracer, ethyl formate, is predominantly controlled by the change in salinity, temperatures, type of electrolytes and EACN, as observed for other reactive tracer candidates. In addition, based on the hydrolysis rate of ethyl formate under site-specific reservoir conditions, the appropriate range of shut-in time can be pre-determined quite confidently before initiating the field test. We believe that the ability of better understanding the partition coefficients and predicting the proper shut-in time beforehand could drastically reduce the risks and uncertainty of SWCTT operations in the field.

References

[1]. Deans, H.A. and Carlisle, C., The single well chemical tracer test a method for measuring reservoir fluid saturations in-situ. pp 615-649, Petroleum Engineering

[2]. Handbook by L. W. Lake (Ed), Vol. 5 Reservoir Engineering and Petrophysics. SPE 2007.

[3]. Huseby, O., Sagen, J. and Dugstad, Ø., Single well chemical tracer tests – Fast and Accurate simulations, SPE 155608, SPE EOR conference at Oil and West Asia held in Muscat, Oman, 16-18 April 2012.

[4]. Chavez, N., Shiau, B., and Harwell, J., Effect of neutral salts and temperature on the partitioning coefficient of ethyl formate used for enhanced oil recovery assessment, SPE 154336, SPE Improved Oil Recovery Symposium in Tulsa, Oklahoma, USA, 14-18 April 2012.

[5]. Vollhardt, P., and Schore, N., Organic chemistry (Structure and Function) 6th ed. pp 936-942, W. H. Freeman and Company, New York, NY 2009.

[6]. Charlisle, C. and Kapoor, S., Development of a rapid and accurate method for determining partition coefficients of chemical tracers between oils and brines (for single-well chemical tracer tests), contract No. DOE/BC/10100-4, U.S. DOE, Washington DC, December 1982.

[7]. Mechergui, A., Romero, C. and Morel, D., Feasibility study of single well tracer test for high salinity and high temperature reservoirs, SPE 161618, Petroleum Exhibition & Conference held in Abu Dhabi, UAE, 11-14 November 2012.

[8]. Tomich, J., Dalton, R. and Deans, H., Single-well tracer method to measure residual oil saturation, SPE 3172, The Journal of Petroleum Technology, Feb. 1973

[9]. Thal, A. E. Jr, Knox, R. C. and Sabatini, D. A., Estimating Partition Coefficients of Tracers, pp 135-142, Ground Water Monitoring & Remediation 27, No. 4, Fall 2007

[10]. Wu, B., and Sabatini, D. A., Using partitioning alcohol tracers to estimate hydrophobicity of high molecular weight LNAPLs, pp 4701-4707, Environmental Science and Technology 34, No. 22, 2000.

[11]. Dwarakanath, V., and Pope, G. A., New approach for estimating alcohol partition coefficients between nonaqueous phase liquids and water. Environmental Science and Technology 32, No. 1: 1662-1666, 1998.

[12]. Deans, H. A., and Carlisle, C. T., Single well tracer test in complex pore systems, SPE/DOE 14886, SPE/DOE Fifth Symposium Enhanced Oil recovery held in Tulsa, OK, April 20-23, 1986.

[13]. Bragg, J. R., Carlson, L. O. and Atterbury, J. H., Recent applications of the single well tracer method for measuring residual oil saturation, SPE 5805, SPE Improved oil recovery symposium of the society of petroleum engineers of AIME held in Tulsa, OK, March 22-24, 1976.

[14]. Chen, J. H., and Adelman, S. A., "Macroscopic Model for Solvated Ion Dynamics," Journal of Chemical Physics, Volume 72, 2819, 1980.

[15]. Shannon, R. D., "Revised Effective Ionic Radii and Systematic Studies of Interatomic Distances in Halides and Chalcogenides," Acta Crystallographica, A32: 751–767, 1976.

[16]. Zangi, R. and Berne, B. J., "Aggregation and Dispersion of Small Hydrophobic Particles in Aqueous Electrolyte Solutions," The Journal of Physical Chemistry, Volume 10, 22736-22741, 2006.

[17]. Burgess, J., "Ions in Solution, Basic Principles of Chemical Interactions," pp. 32-35, Ellis Horwood Limited, Chichester, West Sussex, England, 1988.

[18]. Burgess, J., "Metal Ions in Solution," pp. 20, Ellis Horwood Limited, Chichester, West Sussex, England, 1978.

[19]. Chavez, N., Effect of Neutral Salts on the Partitioning Coefficient and Hydrolysis Reaction of Ethyl Formate Used for Enhanced Oil Recovery Assessment. Master Thesis. 2012

[20]. Tian, W., Estimation of Hydraulic Fracture Volume Utilizing Partitioning Chemical Tracer in Shale Gas Formation, Journal of Natural Gas Science and Engineering, (2016) 1-9

Chapter 2. Enhancing Foam Stability in Porous Media by Applying Nanoparticles

2.1 Introduction

Currently, EOR is responsible for nearly 9% of the oil produced in the world. And virtually, about 70% of worldwide EOR production comes from injecting gases, primarily steam and CO_2, into oil reservoirs. Both steam and CO_2 processes can be efficient within rock strata where the gases contact oil. However, in practice, oil recoveries from field applications are much lower due primarily to poor sweep efficiency. It means that the gas contacts and sweeps only a small portion of the reservoir of its oil. Three major causes of poor sweep efficiency are the low viscosity of injected gases causing fingering, low density of injected gases causing gravity override and geological differences between reservoir layers. (Rossen, 1996).

Foam can improve the sweep efficiency of injected gas by mitigating fingering and gravity override. The mechanism is to increase the displacing fluid viscosity and density for making a more favorable mobility ratio. In other words, foam is a means for mobility control in gas flooding. Also, another mechanism is that foam can block high permeability layers in the reservoir thus divert displacing fluid to lower permeability zones. Moreover, the gas is in more contact with the oil when foam is developed and interfacial mass transfer between the oil and gas will play an important role in oil mobilizing (Horjen, 2015).

Understanding the mechanism of foam generation and propagation in porous media is important for finding the most effective foam assisted EOR processes. Investigation of foam behavior plays crucial roles in understanding the mechanism of foam and

describes the foam ability in porous media. Surfactants have been added to the liquid phase for foam generation for long history. Abbott summarized three reasons of surfactants helping to create foams (Abbott, 2016). In foam flooding technique, polymer is normally used to stabilize the foams, due to modification of viscoelasticity of the interface of foam solution (Wang et al., 2015). Several researchers have conducted experimental studies to assess polymers exceptional benefit of promotion high effective viscosities and stability in bulk foam solution and in sand packs (Sydansk, 1994; Hou et al., 2014; Zhang et al., 2015). However, even the best formulation has the disadvantage that surfactants and polymers can desorb from the interface and adsorb onto the porous medium surface, leaving behind the coarse foam (Prigiobbe et al., 2015). Also, chemistry related issue limits foams stabilized by surfactants at high salinity of the hydrocarbon reservoirs. Anionic surfactants are known to precipitate in aqueous phase with high salinity because they react with multivalent ions. Moreover, foams stabilized by surfactants and polymers have a short lifetime in the presence of oil (Farajzadeh, 2012).

Carbon nanotubes are widely used in human daily life, especially in electrochemical products and sensing applications (Paradise et al., 2007). In recent years, its application has been extended in foam flooding to stabilize foam in porous media. Studies have shown that by adding nanoparticles to bulk foam and porous media, its stability can be considerably strengthened. Singh (2015) reported that fly ash nanoparticle could be used to boost the performance of surfactant-stabilized foams in Berea core for CO_2 EOR mobility control. Prigiobbe et al. (2015) has shown that silica nanoparticles and surfactants stabilized CO_2-foam generated high quality foam in glass bead pack.

Experiments of transport of foam in porous media have also demonstrated that nanoparticles enhance foam stability because they are stable in a wide range of physicochemical conditions (Yu et al. 2014). In this study, multi-walled carbon nanotubes (MWCNT) was applied. Hydrophobic surface of MWCNT can be adsorbed at the liquid/gas interface and behave like surfactant micelles. In an aqueous solution, the hydrophobic surfactant tails adsorb onto the hydrophobic nanotube surface while the hydrophilic surfactant heads point towards the aqueous solution. MWCNTs have a high specific surface area of up to 350 m^2/g, which can provide high adsorption sites for surfactants (Marissa, 2015).

Foam is produced when gas in invaded beneath the surface of a liquid that expands to enclose the gas with a film of liquid. Foam has hexagonal structure of gas cells whose walls consist of lamellae with approximately plane parallel sides. When three or more gas bubbles meet, the lamellae are curved forming the plateau border.

The definition of foam in porous media is that a dispersion of gas in a liquid such that the liquid phase is interconnected and at least some of the gas flow paths blocked by lamellae (Rossen 1996; Falls 1988). This definition includes both bulk foams and individual-lamellae foams (Hirasaki 1985). When foam exists as bulk foam, the average bubble size is much smaller than the dimensions of the pore space, commonly encountered as dishwashing suds and shaving creams. Foam restricted inside a pore network in a porous medium differs from that of "bulk" foams. Individual bubbles of gas separated by lamellae form the confined foam, in which the capillary radius, R, is much less than the equivalent bubble radius, r_b (Falls 1988; Horjen 2015).

Gas and liquid injected in a porous media undergo constantly dynamic mechanisms of in-situ lamella creation and coalescence. The process of lamella creation is a necessary step in foam generation. There is plenty of literature about three fundamental mechanisms for lamella creation in porous media: leave-behind, snap-off and lamella division (Ransohoff and Radke 1988; Falls 1988; Hirasaki 1985; Rossen 1996; Kovscek 1994). Therefore, this study does not further discuss the three fundamental mechanisms. This work reports laboratory experiments in Ottawa sand pack for *in-situ* foam generation using surfactants, polymers and hydrophobic nanoparticles as foam agents in co-injection with air. Through sensitivity analyses, foam quality and stability have been investigated in the study. It helps to understand the mechanism of foam generation and propagation in porous media better.

2.2 Materials

2.2.1 Nanoparticles

In this work, MWCNTs used were supplied by US Research Nanomaterials, Inc. in Houston, TX. We call the MWCNTs US Nano, which has a carbon purity of 99wt%, a median outer diameter of 10nm, a median inner diameter of 4nm, and a median tube length of 2 nm.

2.2.2 Surfactants

Surfactants can act as foam agents. The two surfactants used were a nonionic linear secondary alcohol ethoxylate surfactant called Tergitol 15-s-40 and an anionic alpha olefin sulfonate surfactant called Polystep A-18. Tergitol 15-s-40 is 100 wt% active and was obtained from the Dow Chemical Company. It contains 40 ethylene oxide (EO) groups. Nonionics are generally more tolerant of high salinities than anionics, making

this solution viable in reservoir conditions (Lake, 1989). Polystep A-18 is 39 wt% active and was supplied by Stepan Company. It has a molecular weight of 313 g/mol, and contains an alkyl chain of 14-16 carbons. It exhibits comparatively lower adsorption on sandstones and generates appreciable amount of foam with gas even when the porous medium is partially saturated with oil (Farajzadeh, 2008). Structures of the nonionic and anionic surfactants are shown in Table 2.1, Figure 2.1, and Figure 2.2.

2.2.3 Polymers

Polymer is commonly understood to mean a large molecule composed of repeating units connected by covalent bonds. Polymer has been applied in both the environmental remediation and petroleum industries to alter viscosity, improve sweep efficiency, and enhance the recovery of organic liquids from various geological formations (Anthony et al., 2016). The two polymers used were Xanthan Gum supplied by CP Kelco and HEC-10. HEC-10 is 86 wt% active and was purchased from Sigma Aldrich. Xanthan Gum, which is commonly used in the food industry as a food additive and a stabilizer, is produced by the fermentation of glucose, sucrose or lactose. HEC-10 is used as a viscosity modifier and stabilization agent in a variety of industries ranging from beauty products to oil and gas production. The details about polymers are shown in Table 2.1.

Table 2.1 Detailed Information of Chemicals

Chemical	Trade Name	Type	Formula
Linear secondary alcohol ethoxylate	Tergitol 15-S-40	Nonionic	$C_{11\text{-}15}H_{23\text{-}31}O(CH_2CH_2O)_xH$
Alpha olefin sulfonate	Polystep A-18	Anionic	$C_nH_{2n\text{-}1}SO_3Na$ (n= 14 - 16)
Hydroxyethyl cellulose	HEC-10	Polymer	$[C_6H_7O_2(OH)_{3\text{-}x}[OCH(OH)CH_3]_x]_n$
Xanthan gum	-	Polymer	$C_{35}H_{49}O_{29}$

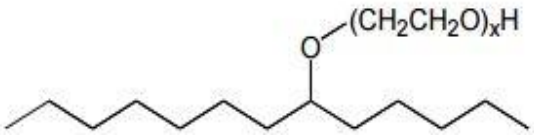

Figure 2.1 Structure of Tergitol 15-S-40 (x = 40)

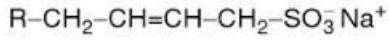

Figure 2.2 Structure of Polystep A-18

2.3 Methods

2.3.1 Stability Test

Preparing a stable MWCNTs dispersion in 3% API brine condition is the first challenge in this study. To prevent adsorption and aggregation of the nanotubes, the particles need to be coated with special chemicals to change their surface properties. In this work, using non-ionic surfactant such as Tergitol-15-S-40 (the detailed information is shown in Table 2.1 & Fig. 2.1) in dispersing MWCNTs in 3% API brine (NaCl: 2.4wt%, $CaCl_2$: 0.6wt %) was found to be successful in producing stable dispersion that can remain stable for several months. The nonionic surfactant is not sensitive to salinity change because it relies on steric repulsion to disperse MWCNTs. This is the reason to make nonionic surfactants as good candidates for high salinity conditions. The hydrophobic tail of the nonionic surfactant is non-covalently adsorbed in the MWCNTs surface, while the hydrophilic head creates steric repulsion to prevent aggregation and improve MWCNTs dispersity (Chen, 2014).

Some researchers demonstrated that polymer is able to facilitate dispersion of nanoparticles in deionized water and high salinity brine except for stabilization foams and modification of viscoelasticity (Kadhum, 2013; Anthony et al., 2016). In high saline conditions, hydroxyethyl cellulose (HEC-10) can be used as a secondary salt tolerant dispersant. Moreover, polymer has the ability to enhance the transport of nanoparticles in sandpacks. The studies conducted by Anthony et al. (2016) reported that a pre-flooding column by HEC-10 improved mobility with 92% effluent recovery of the injected nanoparticles mass. The reason is that the adsorption of HEC-10 on solid phase served to block nanoparticle attachment sites.

The method of ultrasonic was demonstrated to be a preferred method to disperse the MWCNTs in the solution (Dassicos, 2015; Strano et al., 2003). In this study, three stable solutions with dispersing MWCNTs are investigated and analyzed, see Table 2.2.

Table 2.2 Detailed Information of the formulations used in the experiments

Formulation I	Formulation II	Formulation III
Tergitol 15-S-40: 0.2wt%	Tergitol 15-S-40: 0.2wt%	Tergitol 15-S-40: 0.2wt%
		Polystep A-18: 0.2wt%
Polystep A-18: 0.2wt%	Polystep A-18: 0.2wt%	HEC-10: 0.08wt%
Xanthan gum: 0.05wt%	HEC-10: 0.08wt%	Xanthan gum: 0.05wt%
MWCNT: 0.01wt%	MWCNT: 0.01wt%	MWCNT: 0.01wt%

The stable MWCNTs dispersion was first prepared by dissolving Tergitol-15-S-40 in 3% API brine. This solution was stirred with a magnetic stirring bar until the surfactant dissolved completely. Once Tergitol-15-S-40 in 3% API brine was prepared, 0.01wt% (100ppm) MWCNTs was added. The solution was sonicated in a 120-mL glass bottle using a $\frac{1}{2}''$ tip diameter probe sonicator for 35 minutes at 25% amplitude to disperse the MWCNTs in solution. For each formulation, the other chemicals (i.e. Polystep A-18

and Xanthan gum of Formulation I) were added in the solution after primary sonication. After that, the solution was sonicated under same conditions for 10 minutes. The nano-dispersion was then centrifuged for 30 minutes at 2000 rpm to separate the large MWCNT aggregates that did not disperse evenly into the solution after sonication. Subsequently, the nano-dispersion was filtered through 1 μm glass fiber filters. The filtrate was then analyzed by spectrophotometer (UV-vis) at a wavelength of 800 nm to determine the concentration of MWCNTs.

2.3.2 Viscosity Test

In this study, three formulations (Table. 2.2) examined by stability tests were used in the experiments. The viscosities of three formulations without MWCNTs were also examined. A low viscosity rotational type viscometer (LVDV-II Pro, Brookfield Engineering Laboratories, Inc., USA) was used to measure viscosity characteristic of MWCNTs based nanofluids and aqueous fluids. In order to verify the accuracy of the instrument, the viscosity of the pure distilled water was measured prior to experiments. The result is compared with that from the literature. Measurements were taken at several shear rates at 25 ℃.

2.3.3 Setup and Foam Flooding Test

The setup used to carry out the in-situ foam flooding experiments is shown in Fig. 2.3. The setup consists of compressed air tank, mass flow controller, humidifier, syringe pump, glass chromatography column and effluent collector. Ottawa sand was dry packed in 6-inch glass chromatography column purchased from Kimble Chase®. All experiments were run in 3-inch length by 1-inch diameter sandpack. Physical properties of the sandpack are provided in Table 2.3.

Table 2.3 Physical properties of Ottawa sandpack used in the foam flooding experiments

Length (inch)	Diameter (inch)	Porosity (%)	Permeability Darcies
3	1	37.5	4

To conduct the in-situ foam flooding experiments, the dry sandpack was flushed with 3 PV of 3% API brine at a flow rate of 0.3 mL/min to displace any air present and thus ensuring a complete saturation. Liquid solution filled in a syringe pump (Model NE-1000) purchased from New Era Pump Systems Inc. and fed into the bottom of glass column through a valve. Meanwhile, compressed air provided by Airgas® passed through the mass flow controller (Model FMA5504 0-20 mL/min) purchased from Omega® to set a constant air flow rate. A humidifier made by a segment of stainless steel tube located downstream of the mass flow controller. The purpose of using a humidifier is to injected wet air into glass column to prevent precipitation of MWCNTs on the frit. Then wet air entered through the bottom of the glass column as well. To detect the pressure drop during tests, the inlet of the glass column was connected to a pressure gauge with outlet exposed to atmosphere. An effluent collector was located downstream of the outlet of the glass column. After each test, the effluent was used to determine MWCNTs loss in the sandpack. Every part in the setup was connected by 1/8-inch plastic tubing. The experiments were carried out at the temperature of 25 ℃.

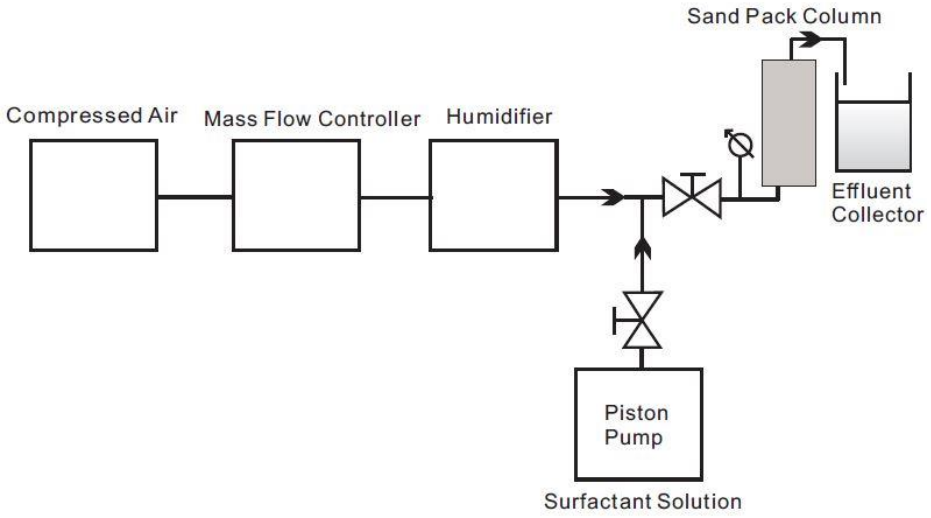

Figure 2.3 schematic of the experimental setup for foam flow in sand column

2.3.4 Foam Quality Test

The foam quality is one of the most important factors affecting foam flow behavior. It is the ratio of gas volume to foam volume (volumetric gas content) at a given pressure and temperature (Grundmann et al., 1983). In a co-injection of gas and liquid strategy, the quality of the foam can be described by the ratio between gas flow rate and total flow rate injected shown in below:

$$Foam\ Quality = \frac{Air\ flow\ rate}{Air\ flow\ rate + liquid\ flow\ rate}$$

Foam quality is closely related to bubble size. As bubble sizes become larger, foam is more likely to be unstable and the foam quality would lower (Sheng, 2013). It typically ranges from 75% to 99%. In this experiment, the effect of foam quality on pressure drop across the sand pack was investigated. The foam quality was changed by varying air flow rates at the constant liquid flow rate. Table 2.4 shows different foam quality of foam agent solution conducted in foam flooding stage.

Table 2.4 Different foam qualities according to different air flow rates with the constant liquid flow rate

Foam Quality	L flow R, ml/min	G flow R, ml/min
90%	0.3	2.7
96.3%	0.3	8
99%	0.3	20

Formulation III was used in the experiment and all of conditions and operations are the same as the foam flooding experiments as mentioned above.

2.4 Results and Discussion

2.4.1 Stability Test

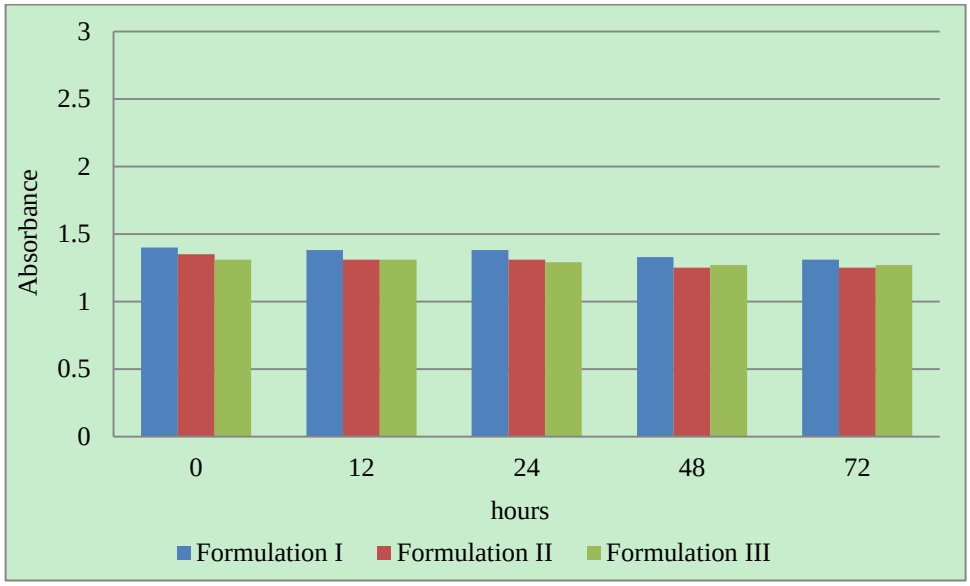

Figure 2.4 72 hours of stability of three formulations with MWCNT dispersion at room temperature, 25 ℃.

As seen in Fig. 2.4, the stability for three formulations is well maintained during the observation period, which demonstrates the effectiveness of surfactants mixed with the polymer stabilized MWCNT dispersions. Through absorbance results of three formulations are compared with the standard calibration curve to determine the

concentrations of MWCNT in 72 hours. The result of MWCNT concentration is shown in Table. 2.5.

Table 2.5 MWCNT concentrations of three formulations in 72 hours

Formulation	conc.(0h), mg/L	conc.(12h), mg/L	conc.(24h), mg/L	conc.(48h), mg/L	conc.(72h), mg/L
I	64	63	63	61	60
II	62	60	60	58	58
III	60	60	59	58	58

As seen in Table.2.5, the nanodispesions meet at least 50% retention of the prepared concentration after the 1 μm filter. Stable dispersions are achieved. After 72 hours, the specimens are then used for the given experiments.

2.4.2 Viscosity Test

The viscosity of nano-dispersions is an inherent property for applications regarding to fluid flow. Better understanding on the characteristic of nano-dispersions' viscosity can reveal the interactions of different chemicals within solution. Viscosity is expressed as resistance of fluid to flow when a shearing force is applied to any deformation. Many fundamental researches over past decade have shown that nanofluids exhibit pseudo-plastic type of non-Newtonian behavior. The pseudo-plastic behavior, "shear thinning" is characterized by a reduction in viscosity of the sample with increasing shear rate. Garg and co-workers (Garg et al., 2009) studied the effect of ultrasonication on viscosity of MWCNT based aqueous nanofluids. They conducted the experiments of nanofluids under 0.5 wt. % MWCNTs mixed with 0.25 wt. % gum arabic (GA) for varying sonication times including 20, 40, 60, and 80 mins and temperature at 15 ℃ and 30 ℃, respectively. Their results clearly showed that MWCNT aqueous nanofluids displayed a non-Newtonian behavior especially at 15 ℃. A shear thinning was observed

resulting in a decrease in viscosity with an increase in shear rate up to 60 s^{-1}, while a slight shear thickening can be observed at 75 s^{-1}. Rheological and thermal conductivity studies of Sadri et al. (Sadri et al., 2014) has demonstrated the shearing thinning behavior of 0.5 wt. % MWCNTs and 0.25 wt. % GA at 15 ℃, 30 ℃, and 45 ℃. He found that the viscosity of nanofluids shows a sharp decrease with increase of shear rate at lower shear rates, where for shear rates at higher the viscosity becomes gradually constant. The shear thinning behavior of MWCNT nanofluids was also observed by Ponmozhi (Ponmozhi et al., 2010). They reported that the viscosity of nanofluids increases significantly for a small increase of MWCNT concentration and it decreases with temperature rise.

In this study, the viscosities of MWCNT based nanofluids stabilized by Tergitol-15-s-40 dispersant and mixed by other chemicals were measured as a function of shear rate. Figs. 2.5 a, b, c shows the results for nanofluids of Formulation I, Formulation II and Formulation III and aqueous fluids, respectively.

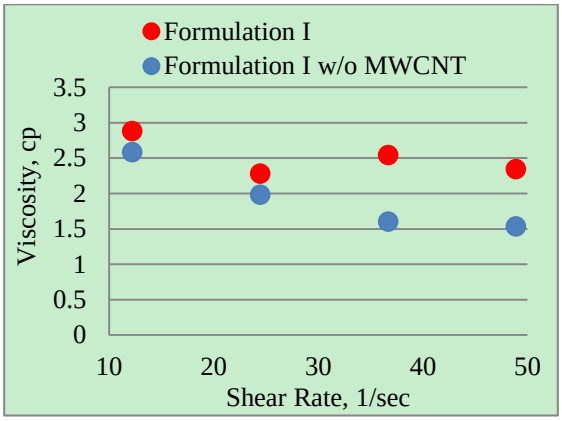

(a)

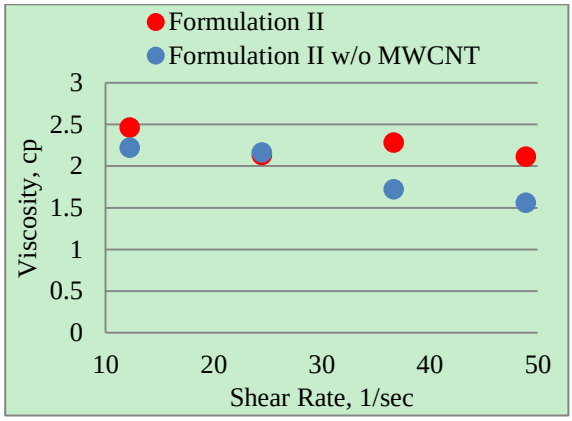

(b)

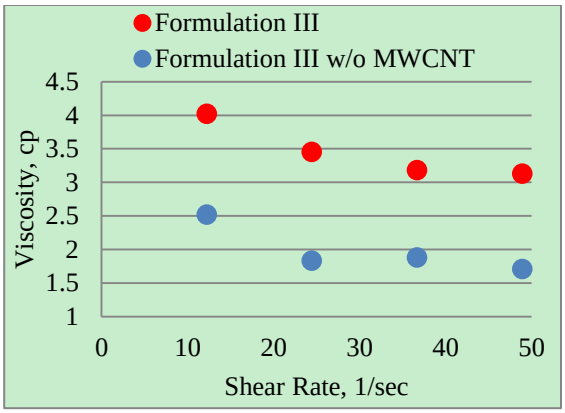

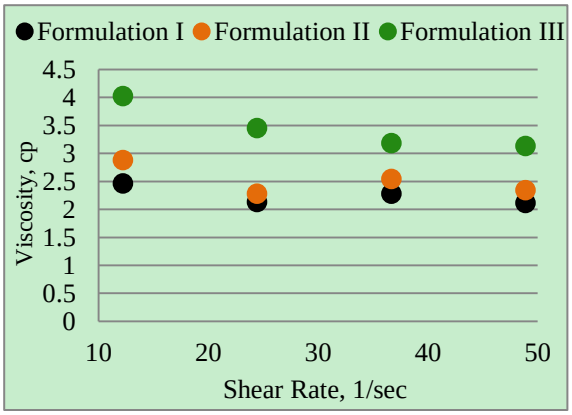

(c) (d)

Figure 2.5 **Variation of viscosity as function of shear rate at 25 ℃. (a) Formulation I and Formulation I w/o MWCNT. (b) Formulation II and Formulation II w/o MWCNT. (c) Formulation III and Formulation III w/o MWCNT. (d) A comparison among Formulation I, Formulation II and Formulation III**

It is obvious from the Fig 2.5. a), b), c) that the nanofluids behave as a non-Newtonian fluid because the dynamic viscosities varies accordingly with an increase shear rate. A shear-thinning trend of MWCNT nanofluids was also observed through Fig 2.5, which has been confirmed once again. Figs. 2.5. a), b), c) also shows that the viscosity of MWCNT nanofluids is higher than that of aqueous fluids at the same concentration. Addition of MWCNTs into aqueous fluids displays high viscosity due to surfactant is capable of modifying nanotube's surface from hydrophobic to hydrophilic resulted in an increase in repulsive force among the nanotubes. Thus, the surface area of well dispersed MWCNTs nanofluids increases. Particles agglomeration that reduced by the addition of surfactant resists fluid to flow resulted in an increment in viscosity of nanofluids. The viscosities of three Formulations with MWCNT dispersions at similar concentration are plotted versus different shear rates in Fig. 2.5. d). It is seen that the viscosity of Formulation III has higher viscosity compared to that of Formulation I and

II. A slight higher viscosity can be attributed to the properties of Xanthan Gum which has shown high resistance at low shear rates in past studies (Zatz et al., 1982).

2.4.3 Foam Flooding Experiments

After the 3-inch sandpack completely saturated by 3 PV (1 pore volume=13.5ml) of 3% API brine at a flow rate of 0.3 ml/min, the sandpack was flushed with a 3 PV pre-flushed solution comprised of 0.08 wt% HEC-10 prepared in 3% API brine. Addition of HEC-10 in based 3% API brine is to reduce surfactant adsorption in porous media. As seen in Fig. 2.6, before the first dash line, it shows Δp during the process of the 3 PV pre-flushed solution. Subsequently, the liquid solution prepared according to Formulation I was injected into the sandpack at a constant flow rate of 0.3 mL/min, meanwhile, the air was co-injected directly into the saturated sandpack at fixed rate 8mL/min. The Δp for the co-injected stage was presented in Fig. 2.6 as well, which located between the first dash and the second dash line. In Fig. 2.6, the black circle and red triangle were used to represent the foam breakthrough from the sandpack. The black one is located in blue curve and the red triangle is located in the pressure drop of the solution without MWCNTs. In the co-injected stage, Δp increases smoothly while the foam forms until post-flushed stage. It increases at around a constant value while approaching steady state (Gauglitz et al., 2002). The foam, therefore, is stable and was considered as strong foam. The last part in Fig. 2.6 is the recorded pressure drop of post-flushed solution, which was only prepared by 3% API brine. In the post-flushed stage, injection of the air was ceased and the flow rate of 3% API brine injected was consistent with the flow rates of the first two stages. The purpose of post-flushed

solution injected is to observe a slump in the pressure drop. It means that the foam agent solution did not occur to agglomerates in porous media to block the sandpack.

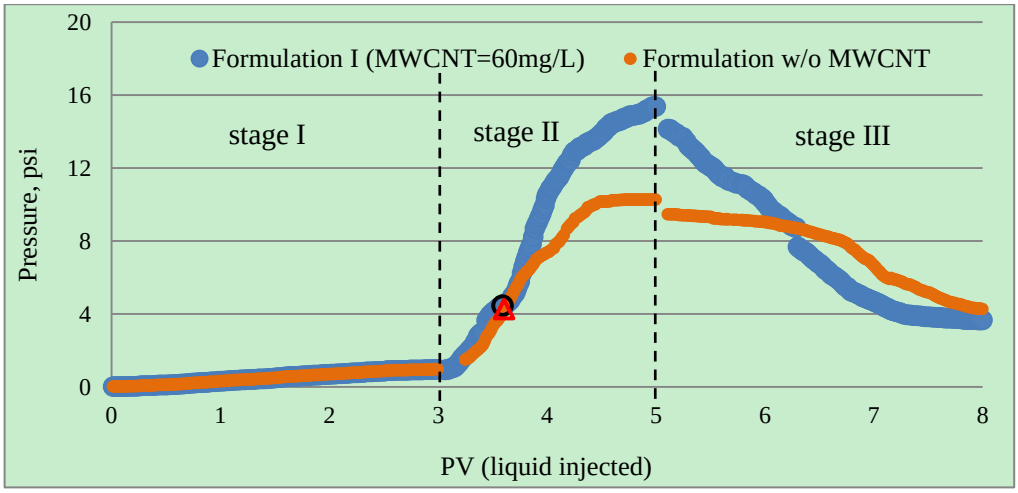

Figure 2.6 Pressure drop (Formulation I) as a function of pore volume of liquid injected

Foam was formed in the sandpack and collected at regular intervals. The effluent which was in the form of foam was allowed to collapse and then the concentration of MWCNTs measured by UV-Vis as shown in Fig. 2.7. The ratio of C to C_0 is the proportion of the concentration of MWCNTs in effluent to the concentration of MWCNTs at initial injection. Since the first three PVs is pre-flush stage that the injected solution did not introduce MWCNTs, the sandpack and effluent did not contain any MWCNTs as well. Therefore, the concentration of MWCNTs was detected only at foam flooding and post-flushed stages. As seen in Fig. 2.7, initially, the concentration of MWCNTs in the effluent sample is around 0 results in the ratio of C to C_0 at 0 as well. Once the foam broke through the sandpack, the MWCNTs could be detected in the effluent samples. The maximum C/C_0 achieved 0.72 at 4.38PV. For Formulation I, only by 1.38PV, the maximum C/C_0 could be observed. And the C/C_0 value maintained at high level from 4PV to 5PV. It means that MWCNTs stably migrated in the sandpack.

Followed by 2 PVs foam flooding injected, 3 PVs post-flushed solution was injected into the sandpack. Since the post-flushed solution contained only 3% API brine and injection of the air was ceased, the pressure drop decreased gradually. As a result, the concentration of MWCNTs in effluent samples fell off quickly until to 0.

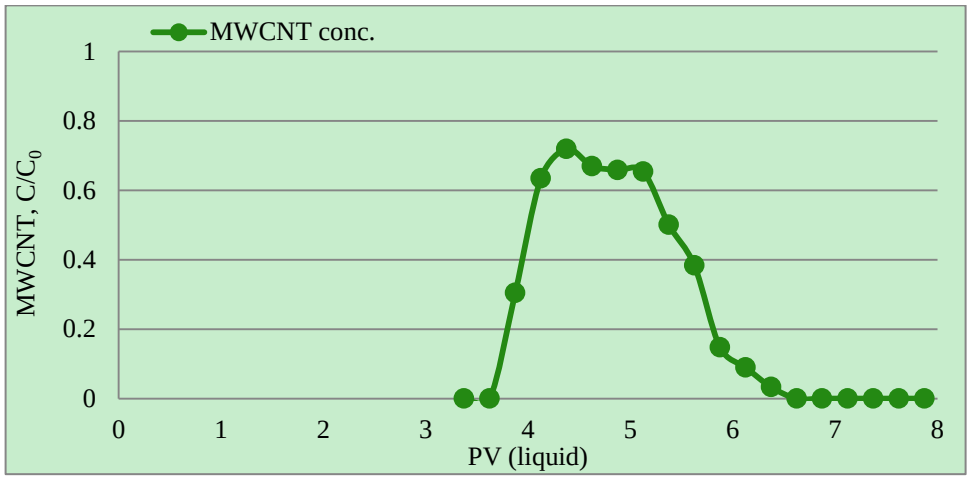

Figure 2.7 **WCNTs conc. in each effluent sample from sandpack for formulation I**

Fig 2.8. and Fig 2.9. are the results of the experiment for Formulation II. All of conditions and operations are the same as the above experiment of Formulation I. The only difference is that the Formulation I used as foam agent solution was replaced with Formulation III. As seen in Fig 2.8., the maximum pressure drop of the experiment of Formulation II is lower than that of the experiment of Formulation I because the properties of xanthan gum and HEC-10 are different. The viscosity range of Xanthan Gum at 1 wt% is narrower than that of HEC-10 at the same weight percentage. Also, the concentration of HEC-10 in formulation II is higher than the concentration of Xanthan Gum in formulation I. Since HEC-10 is capable of reducing surfactant adsorption in the sandpack, it is beneficial to discharging more MWCNTs to the effluent collectors.

Therefore, in Fig.2.9, its C/C_0 value at foam flooding stage is higher than the value at the same stage of the experiment of Formulation I.

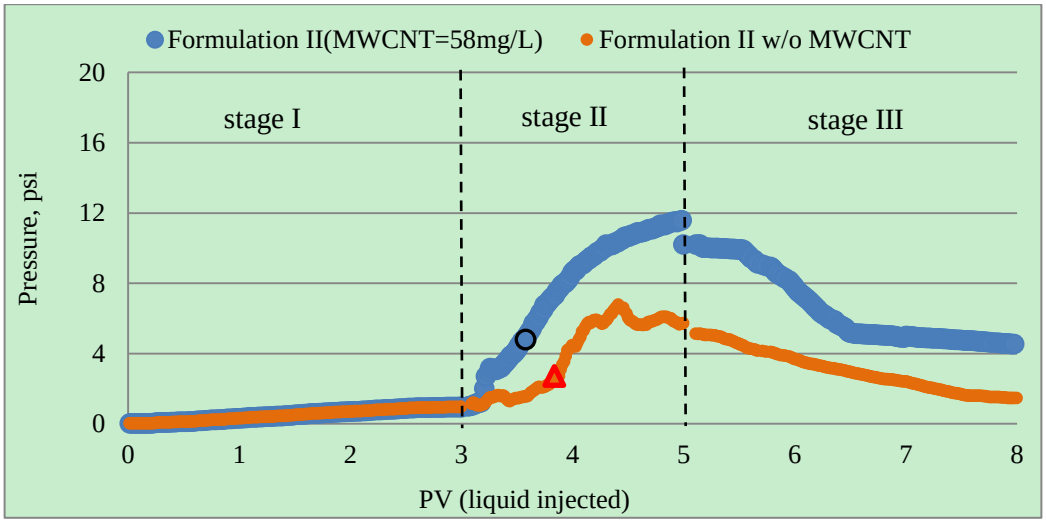

Figure 2.8 Pressure drop (Formulation II) as a function of pore volume of liquid injected

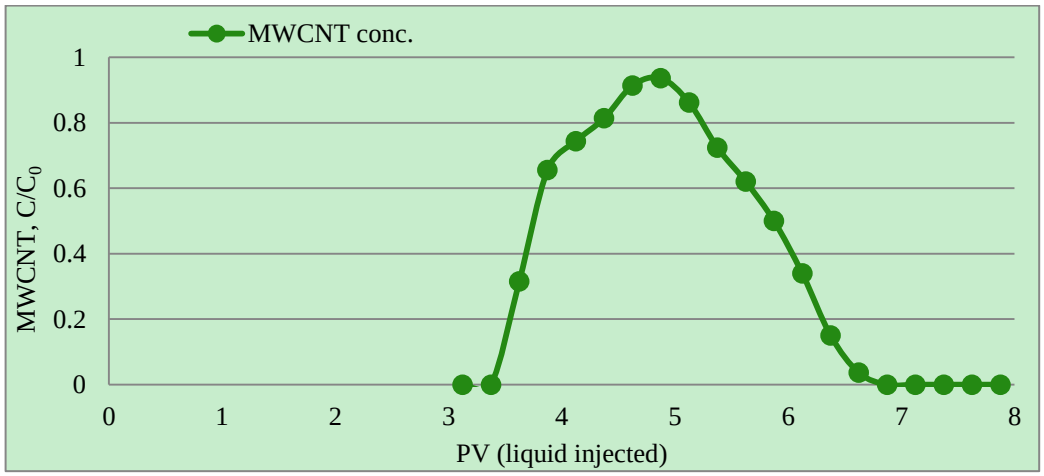

Figure 2.9 MWCNTs conc. in each effluent sample from sandpack for formulation II

Fig 2.10 and Fig 2.11 are the results of the experiment for Formulation III. The experiment has the same conditions and operations with the pervious experiments. The difference is that the performance of Formulation III was investigated in the experiment. Since the viscosity of Formulation III was higher than the others' (see Fig

2.5(d)), the pressure drop of the experiment of Formulation III achieved 19 psi in the foam flooding stage. Compared with the pressure drops of the above experiments, the pressure change of the experiment of Formulation III is significantly higher. In Fig 2.10, the foam breakthrough time of the experiment of Formulation III is prior to that of the experiments of Formulation II and Formulation I. As seen in Fig 2.11, the C/C_0 value of the experiment of Formulation III does not show too much difference with the value of the experiment of Formulation I.

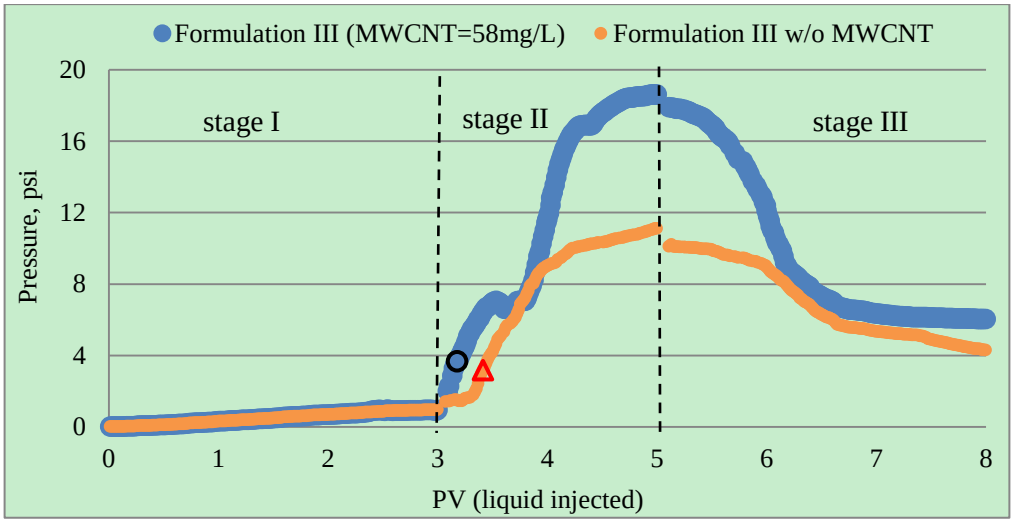

Figure 2.10 Pressure drop (Formulation III) as a function of pore volume of liquid injected

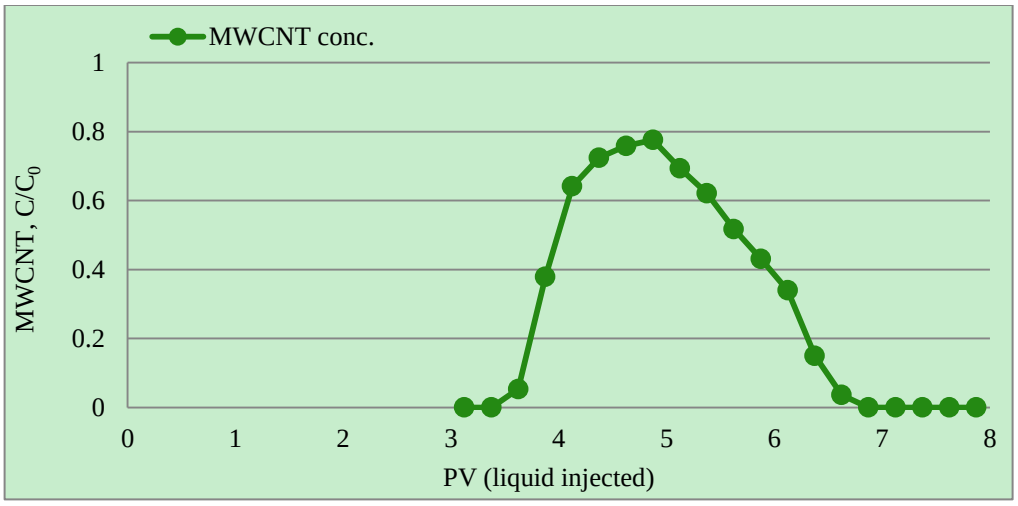

Figure 2.11 MWCNTs conc. in each effluent sample from the sandpack for formulation III

Studies have shown that by dispersing MWCNTs in surfactant and polymer solutions, the stability and microstructure of produced foam can be further considerably increased (Krämer et al., 2016). Experiments of transport of foam in a porous medium have also demonstrated that nanoparticles improve foam propagation and stability (Yu et al. 2013; Sun et al. 2014; Valentina et al. 2015). MWCNTs are adsorbed at liquid/air interface preserving the foam texture, which reduces the drainage within the lamella. Simultaneously, MWCNTs decrease the gas diffusion through the thin film providing a barrier for bubble coalescence. . Moreover, large adsorption sites on MWCNTs surface enables it to adsorb huge amount of surfactant molecules hence lowers surfactant molecules adsorbed on the surface of porous medium as a result of competitive adsorption. Thus, fewer molecules are available for formation of micelles and the degree of hydrophobic property of MWCNTs decreases so that a super micelle is formed in the lamella (Fig.2.12(a)). The super micelle creates an armor which dramatically reduces the liquid drainage and minimizes MWCNTs aggregation.

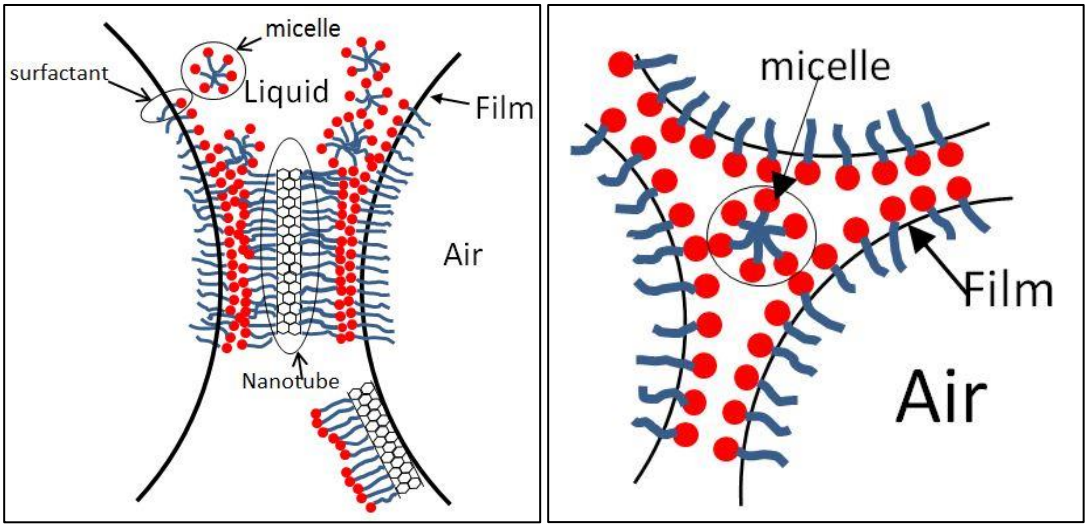

(a) (b)

Figure2.12 Schematic of representation of the surfactant interaction with MWCNTs (a) and without MWCNTs (b) at liquid/air interface.

Except for recording the pressure drop across the sandpack and detecting the concentration of MWCNTs in effluent samples for each experiment, the recovery and loss of MWCNTs in the sandpack for each experiment were investigated as well. The related results are shown in Table.2.6. MWCNTs recovery is measured as a ratio of the total amount of MWCNTs in effluent to the amount of MWCNTs injected (Caldelas et al., 2011). The recovery was further used to calculate the MWCNTs retention per gram of Ottawa sand in 3-inch sandpack. Simple mass balance equations were applied to calculate the recovery and retention. Here the accumulation was considered as retention. All calculations based on amount of liquid present in the foam.

Table 2.6 MWCNT recovery and retention in the sandpack

Formulation	MWCNT Recovery, %	(Mass MWCNT retained)/ (Mass of Sand), (mg/g_{sand})
I	68	0.00627
II	74	0.00702
III	71	0.0075

The results in Table 2.6 do not have huge difference. Typical surfactant adsorption in a sandpack is around 1 mg/g_{sand}. All these values about retention of MWCNTs in the sandpack are less than 0.01 mg/g_{sand}. This is a significant achievement because MWCNTs were capable of travelling throughout the sandpack without becoming trapped.

2.4.4 Effect of foam quality on foam flooding

As seen in Fig 2.13, after the sandpack was pre-flushed by 3 PVs solution comprised of 0.08% HEC-10 prepared in 3% API brine, the air and the foam agent solution with MWCNT simultaneously injected into the sandpack according to different foam quality. 3 PVs of 3% API brine used as post-flushed solution followed the foam flooding stage. In Fig 2.13, the rupture of blue curve between stage II and stage III is due to human error in operations. The results show that increasing the foam quality from 90% to 99%, the pressure drop across the sandpack increase as well. The change radically results from increasing the air flow rate. The foam breakthrough time of each test is different but they were extremely close. All of them could be observed in the first one PV of foam flooding stage.

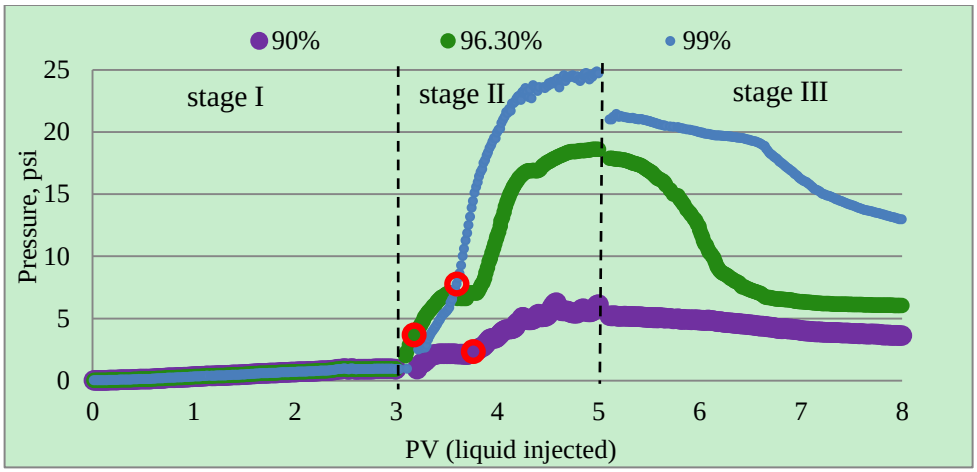

Figure 2.13 Different pressure drop (Formulation III) as a function of liquid PV injected according to varies foam qualities

2.5 Conclusions

In this experimental study, stability and viscosity tests of foam agent solutions, pressure drop across porous media, and foam quality test were performed to study the effect of MWCNTs on surfactant foam solutions for EOR. Conclusions drawn are as follows:

- Foam can be generated using surfactants (Polystep A-18, Tergitol) and polymers (HEC-10, Xanthan gum) without oil in the presence of MWCNTs.
- The formulation III has higher viscosity than the other formulations because of the synergistic effect of xanthan gum and hec-10.
- Foam stability in porous media was measured by simultaneously injecting stabilized foam agent solutions and the air in the sandpack at a constant flow rates. The pressure drop across the sandpack of all tests increased. The experiment of Formulation III gave a higher pressure drop than the others.

- MWCNTs retention in the porous media was measured by conducting mass balance across the sandpack. It is observed that MWCNTs retention per gram of Ottawa sand is lower than the retention of surfactant.
- Foam quality was recognized as an important parameter affecting foam flow behavior. Higher foam quality gave a higher pressure drop. It radically resulted from increasing the air flow rate.
- MWCNT is capable of affecting formability and foam flow behavior in porous media.

References

[1] Rossen, W.R., "Foams in Enhanced Oil Recovery" in R. K. Prud'homme and S. Khan, ed., *Foams: Theory, Measurements and Applications*, Marcel Dekker, New York, 1996, pp. 413-464.

[2] Rosen, M.J.; Kunjappu, J.T. "Characteristic Features of Surfactants" in Melton J. Rosen, ed., *Surfactants and Interfacial Phenomena*, Brooklyn College, New York, 2004, pp. 1-34

[3] Sheng, J.J., "Surfactant Flooding" in J.J. Sheng, ed., *Modern Enhanced Oil Recovery: Theory and Practice,* Burlington, MA, USA, 2011, pp. 239-242

[4] Abbott, S., "Foams" in S. Abbott, ed., *Surfactant Science: Principles & Practice*, Ipswich, UK, 2016, pp. 132-148

[5] Kovscek, A.R.; Radke, C.J., "Fundamentals of foam transport in porous media" in Laurier L. Schramm, ed., *Foams: Fundamentals and Applications in the Petroleum Industry*, Washington, DC, 1994, pp. 115-163

[6] Sheng, J.J., "*Enhanced Oil Recovery Field Case Studies*" Gulf Professional Publishing 24th May, 2013

[7] Prigiobbe, V.; Worthen, A.J.; Johnston, K.P.; Bryant, S.L. 2016. Transport of nanoparticle-stabilized CO_2-foam in porous media. *Transp Porous Med* (2016) 111: 265-285

[8] Yu, J.; Wang, S.; liu N.; Lee, R. 2014. Study of particle structure and hydrophobicity effects on the flow behavior of nanoparticle-stabilized CO_2 foam in porous media. Presented at the SPE Improved Oil Recovery Symposium, Tulsa, Oklahoma, 12-16 April. SPE-169047-MS.

[9] Harris, P. J. F. 2004. Carbon nanotube composites. *International Materials Reviews* 49(1):31-43

[10] Gajewicz, A.; Rasulev, B; Dinadayalane T.C.; Urbaszek, P.; Puzyn, T.; Leszczynska, D.; Leszczynski, J. 2012. Advancing risk assessment of engineered nanomaterials: Application of computational approaches. *Advanced Drug Delivery Reviews* (2012) 64: 1663-1693

[11] Liu, C.L.; Nikas, Y.J.; Blankschtein, D. 1996. Novel bioseparations using two-phase aqueous micellar systems. *Biotechnology and Bioengineering* 52(2): 185-192

[12] Anthony, A.K.,; Becker, M.D.; Lyon, B.A.; Foster, E.; Zheng, X.; Johnston, K.P.; Abriola, L.M.; Pennell, K.D. 2016. Improved mobility of magnetite nanoparticles at high salinity with polymers and surfactants. *Energy & fuels* (2016) 30: 1915-1926

[13] Wang, D.; Hou, Q.; Luo, Y.; Zhu, Y.; Fan, H. 2015. Stability comparison between particles-stabilized foams and polymer stabilized foams. *Journal of Dispersion Science and Technology* (2015) 36: 268-273

[14] Sydansk, R.D. 1994. Polymer-enhanced foams part 1: Laboratory development and evaluation. *SPE Advanced Technology Series* (1994) 2: 150-159

[15] Liu, H.; Wang, J.; Yang, L.; Jiang, D.; Lv, C.; Cui, C.; Gao, S. 2012. Studies on foam flooding EOR technique for Daqing reservoirs after polymer flooding. Presented at the SPE Improved Oil Recovery Symposium, Tulsa, Oklahoma, 14-18 April. SPE-151955-MS.

[16] Zhang, C.; Wang, Z.; Li, J.; Xiong, Z. 2015. The experimental study of foaming system suitable for high temperature foam gas driving. Presented at 4th International conference on sensors, Measurement and intelligent materials (ICSMIM 2015).

[17] Falls, A.H.; Hirasaki, G.J.; Patzek, T.W.; Gauglitz, D.A.; Miller, D.D.; Ratulowski, T. 1988. Development of a Mechanistic Foam simulator: The population balance and generation by snap-off. *SPE Reservoir Engineering Series* (1988) 3: 884-892

[18] Hirasaki, G.J. and Lawson, J.B. 1985. Mechanisms of foam flow in porous media: Apparent viscosity in smooth capillaries. *Society of Petroleum Engineers Journal*(1985). SPE-12129

[19] Ransohoff, T.C. and Radke, C.J. 1988. Mechanisms of foam generation in glass-bead packs. *SPE Reservoir Engineering* (1988) 5: 573-585 SPE-15441-PA

[20] Farajzadeh, R.; Andrianov, A.; Krastev, R.; Hirasaki, G.J.; Rossen, W.R. 2012. Foam-oil interaction in porous media: Implications for foam assisted enhanced oil recovery. *Adv. Colloid Interface Sci.* (2012),183-184, 1-13

[21] Paradise, M. and Goswami, T. 2007. Carbon nanotubes-production and industrial applications. *Materials & Design.* (2007) 28: 1477-1489

[22] Yurekli, K.; Mitchell, C.; Krishnamoorti, R. 2004. Small-Angle neutron scattering from surfactant-assisted aqueous dispersions of carbon nanotubes. *J. AM. Chem. Soc. (2004) 126: 9902-9903*

[23] Krämer, C.; Kowald, T.L.; Butters, V.; Trettin, R.H.F. 2016. Carbon nanotube-stabilized three-phase-foams. *J Mater Sci (2016) 51:3715-3723*

[24] Yu, J.; Mo, D.; Liu, N.; Lee, R. 2013. The application of nanoparticle-stabilized CO_2 foam for oil recovery. Presented at the SPE International Symposium on Oilfield Chemistry held in The Woodlands, Texas, USA 8-10 April 2013.SPE-164074

[25] Sun, Q.; Li, Z.; Jiang, L.; Wang, J.; Wang, P. 2014. Utilization of surfactant-stabilized foam for enhanced oil recovery by adding nanoparticles. *Energy Fuels (2014) 28: 2384-2394*

[26] Strano, M.; Moore, V.C.; Miller, M.K.; Allen, M.J.; Haroz, E.H.; Kittrell, C.; Hauge, R.H.; Smalley, R.E. 2003. The role of surfactant adsorption during ultrasonication in the dispersion of single-walled carbon nanotubes. *Journal of Nanoscience and Nanotechnology, (2003) 3: 81-86*

[27] Dassios, K.; Alafogianni, P.; Antiohos, S.K.; Leptokaridis, C.; Barkoula, N.M.; Matikas, T.E. 2015. Optimization of sonication parameters for homogeneous surfactant-assisted dispersion of multiwalled carbon nanotubes in aqueous solutions. *J. Phys. Chem. C (2015) 119: 7506-7516*

[28] Chen, C.; Kadhum, M.J.; Mercado, M.C.; Shiau, B.; Harwell, J.H. 2016. Surfactant-only stabilized Dispersions of Multiwalled Carbon Nanotubes in High-Electrolyte-Concentration Brines. *Engergy & Fuels (2016) 30(11):8952-8961*

[29] Garg, P.; Alvarado, J.L.; Marsh, C.; Carlson, T.A.; Kessler, D.A.; Annamalai, K. 2009. An experimental study on the effect of ultrasonication on viscosity and heat transfer performance of multi-wall carbon nanotube-based aqueous nanofluids. *Int. J. Heat Mass Transfer (2009) 52: 5090-5101*

[30] Ponmozhi, J.; Gonçalves, F.A.M.M.; Ferreira, A.G.M.; Oliverira, M.S.A. 2010. Thermodynamic and transport properties of CNT water based nanofluids. *J. Nano Res. (2010) 11: 101-106*

[31] Sadri, R.; Ahmadi, G.; Togun, H.; Dahari, M.; Kazi, S.N.; Sadeghinezhad, E.; Zubir, N. 2014. An experimental study on thermal conductivity and viscosity of nanofluids containing carbon nanotubes. *Nanoscale Research Letters (2014) 9: 151*

[32] Zatz, J.; Knapp, S. 1984. Viscosity of xanthan gum solutions at low shear rates. *Journal of Pharmaceutical Sciences (1984) 73(4):468-471*

[33] Grundmann, S. and Lord, D.L. 1983. Foam stimulation. *Journal of Petroleum Technology (1983):597-602*

[34] Caldelas, F.; Murphy, M.; Huh, C.; Bryant, S.L. 2011. *Factors governing distance of nanoparticle propagation in porous media* presented at the SPE Production and Operations Symposium held in Oklahoma City, USA, 27-29 March 2011.

[35] Horjen, H. T., 2015. CO_2 foam stabilization with nanoparticles and EOR in fractured carbonate systems. M.S. Thesis, University of Bergen: Bergen, Norway.

[36] Mercado, M. 2015. Enhanced in-situ carbon nanotubes in high salinity brine. M.S. Thesis, University of Oklahoma: Norman, OK

[37] Kadhum, J. M. 2013. Interfacially active carbon nanotube hybrids for reservoir development applications. PH.D Thesis, University of Oklahoma: Norman, OK.

[38] Farjzadeh, R.; Krastev, R.; Zitha, P.L.J. 2008. Foam films stabilized with alpha olefin sulfonate (AOS). *Colloids and Surfaces A: Physicochem. Eng. Aspects 324 (2008): 35-40*

[40] Lake, L. 1989. Enhanced Oil Recovery, first edition. Englewood Cliffs, New Jersey: Prentice Hall.

[41] Singh, R.; Gupta, A.; Mohanty, K.K.; Huh, C.; Lee, D.;Cho, H. 2015. *Fly ash nanoparticle-stabilized CO_2-in-water foams for gas mobility control applications.* Presented at the SPE annual Technical Conference and Exhibition held in Houston, Texas, USA, 28-30 September 2015.

[42] Gauglitz, P.A.; Friedmann, F.; Kam, S.I.; Rossen, W.R. 2002. Foam generation in homogenous porous media. *Chemical Engineering science 57(2002): 4037-4052*

Chapter 3. Counterion Binding on Coacervation of Aerosol-OT in Aqueous Sodium Chloride

3.1 Introduction

Coacervation is a subtle system in colloid science. It refers to the solution of colloidal molecules that separates from an aqueous solvent for formation of dense phase. Since the dense phase is rich in colloidal or macromolecular components, it is immiscible with relatively poor colloidal dilute liquid phase. The dense phase is called as coacervate. It does not freely mix with the equilibrium aqueous phase. The definition of a coacervate is incompatible with its own solvent (Menger, 1998). There is increasing interest in understanding the formation of coacervate due to the development of applications, such as, cleaning products (Wasilewski, 2010), food formulation (Yeo et al., 2005), drug delivery (Saravanan et al., 2010; Feng et al. 2014), and cosmetic products (Goddard et al., 1990). Simple coacervation involves single colloid species and addition of salt promotes coacervation. In complex coacervation systems, at least two oppositely charged species are involved. Our investigations focus on a simple coacervate, AOT and NaCl in deionized (DI) water. Some great efforts have devoted to study coacervation mechanism (Menger et al., 2001; Imura et al., 2004) and coacervates application (Xiao et al., 2014). However, the coacervates boundary of simple system has not been reported before. Thus, in this work, simple coacervation has been investigated in the NaCl aqueous solution of AOT (dioctyl sulfosuccinate). Additional, the counterion binding constant (β) at coacervates formed in the samples arouses our interest. A lot of literature reported that the profile of β changed in clear colloid solutions. Few researchers worked on the value β above the coacervates boundary.

Therefore, extensive our knowledge to this field is very necessary. This work also involved the evolution of particle size in colloid solutions detected by DLS. The results help further understand the coacervates in simple system.

3.2 Experimental Section

3.2.1 Materials

Anionic surfactant Aerosol OT, supplied by Fisher, is ultra-pure at 99 wt% active. It has a white wax solid appearance. Sodium chloride is 100 wt% active. It was purchased from Sigma Aldrich.

3.2.2 Turbidity Measurement

Turbidity was used to qualitatively measure of the extent of coacervation as a function of salt concentration. According to turbidity measurements, the boundary of coacervates in AOT/NaCl system can be determined. Turbidity measurements were made using a UV spectrophotometer (Genesys 10 S UV-Vis, Thermo Fisher Scientific Inc.). It can determine the extent of turbidity by measuring the amount of light that passed through a specimen. Less light passing through the specimen means more aggregation in the suspension. Turbidity was measured at a wavelength of 550 nm and a temperature of 25 ℃ (Perry et al., 2014). Since at this wavelength AOT does not absorb, the total absorbance is due only to turbidity (Puig et al., 1991). The turbidity of AOT/NaCl solution reported as $-\ln(\%T)$. T is transmittance and expressed by I/I_0, with I_0 = intensity of the incident radiation entering the medium and I = intensity of the transmitted radiation leaving the medium, and is measured in absorption units (a.u.).

3.2.3 Ion Selective Electrode

A specific ion electrode with an Oakton Instruments Inc. digital pH/mV meter, Model PH11 was used to measure EMF data to determine counterion binding constant. For anionic surfactant AOT and NaCl system, an Oakton sodium ion-selective glass body electrode, Model WD-35802-43 was used. The electrode combines reference cell and measuring cell for ease to use. For making EMF measurements as a function of AOT concentration, a volume of 40 mL of water or aqueous NaCl solution of desired concentration and a small magnetic stirring bar were added to the 80-mL beaker thermostated at 25 ℃. The sodium ion selective glass electrode was clamped in an iron support so that the electrode tip was dipped into the aqueous solution to be measured. The solution was continuously stirred by a small magnetic stir bar located under the beaker. After the electrode had equilibrated, successive small aliquots of stock solution of AOT in the electrolytic solution of chosen concentration were added with a Finn pipette (Umlong, et al. 2005; Kalldas, et al. 1980).

3.2.4 Dynamic Light Scattering

The size measurements were performed at 25 ℃ by using dynamic light scattering (DLS) (Brookhaven Instruments Corp, Holtsville, NY) equipped with 532 nm laser at scattering angle of 90 °. The correlation function was analyzed from the scattering data via the NNLS method because there is different sizes distribution in the solutions. The apparent hydrodynamic radius R_h was deduced by the Stokes-Einstein equation $R_h = k_B T/(6\pi\eta D)$ for spherical particles, where k_B represents the Boltzmann constant, T is the absolute temperature, and η is the solvent viscosity. All experiments were performed at 25 ℃ (Wang, et al. 2013; Kelley, et al. 2014).

3.2.5 Preparation of Specimens

A series of samples were prepared by addition of known volumes of NaCl solution of desired concentration to given volumes of aqueous AOT with desired concentration in 40 mL vials. The specific procedure is to set the concentration of NaCl at constant, firstly. A group of aqueous AOT with increment in concentration which is an adequately amount until coacervates can be formed in samples was added into the NaCl solutions at constant concentration. Samples were capped and shaken by hands. Phase separation was considered to be complete when the coacervates were formed and equilibrium liquid remained constant over several days. The group samples presented visual results from clear to turbid. According to turbidity measurements, the boundary can be determined. All experiments were performed at 25 ℃.

3.3 Results and Discussion

3.3.1 Phase Boundary Determination

The critical micellar concentration of AOT is 2.8 mM in deionized water (DI) and the solubility of AOT in DI water is around 28 mM at 25 ℃. So at first, the range of the concentration of AOT selected to study was from 3 mM to 18 mM. The experiments were conducted by keeping AOT concentration at each value of the above range and varying NaCl concentration from low to high until coacervates was formed in the solutions so that the transmittance of samples measured by UV-Vis changes. From Figure 3.1(a) to Figure 3.1(e) show the turbidimetric curves of the AOT concentration from 3 mM to 18 mM with varying NaCl concentrations, respectively, at 25 ℃. All the turbidity curves show a similar changing trend with the increasing NaCl concentration. Thus, phase transition with the increase of NaCl concentration will be discussed by

taking AOT at 3 mM as a representative in the following content. In Figure 3.1(a), the turbidity is closely zero and the solution is optically transparent below 18 mM NaCl concentration. With continuing to add NaCl into the solution to reach 18.5 mM, the turbidity initially stars to increase. This critical NaCl concentration is denoted C, as seen in Figure 3.1(a). The initial turbidity increase at C illustrates the appearance of larger AOT/NaCl aggregates in the solution. Then, with addition of NaCl in the solution, the turbidity dramatically increases and the solution becomes cloudy. The critical NaCl concentration, C, can be determined from the turbidity curves with different AOT concentrations. Through the analysis of the critical NaCl concentration of the turbidity curves at each AOT concentration, the phase boundary of AOT/NaCl derived from Figure 3.1(a) to Figure 3.1(e) and summarized in Figure 3.1(f). The coacervation region is located at upper right. The region located at bottom left is small micelles. The main reason for coacervation formation can be understood in terms of a change in the spontaneous mean curvature. In the absence of NaCl, repulsive electrostatic forces among the headgroups favor a positive mean curvature. When salt is added, the electrostatic contribution to the curvature free energy diminishes, and the mean curvature is driven to negative values. The positive to negative change in the mean curvature has less to do with entropic considerations than with the surfactant seizing the opportunity to obtain optimal curvature. The stronger the binding of Na^+ to the anionic AOT surfactant, the more effective the shielding of the electrostatic repulsion among the anionic headgroups, and the more readily the mean curvature inverts to a negative where the headgroups are more tightly packed. The effective binding of Na^+ to the surface of headgroups permits closer packing of the AOT

sulfonate headgroups. Thus, the mean curvature converted to negative is necessary for coavervate formation (Menger, et al. 1998).

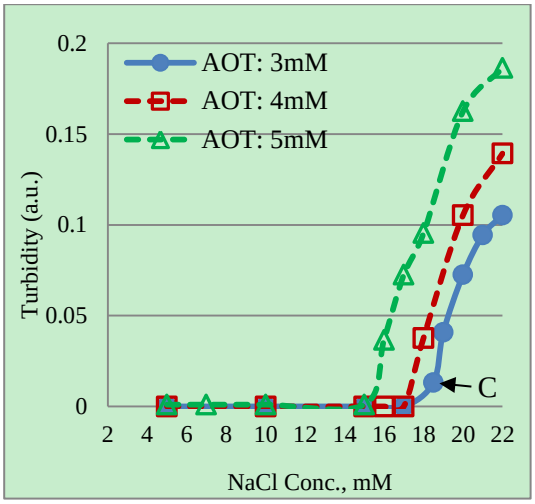

(a)

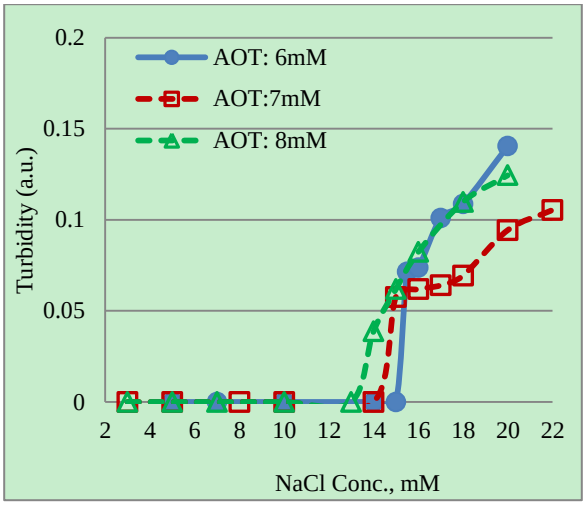

(b)

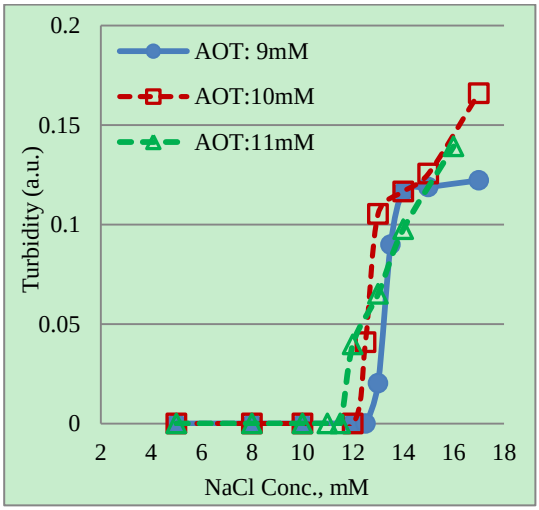

(c)

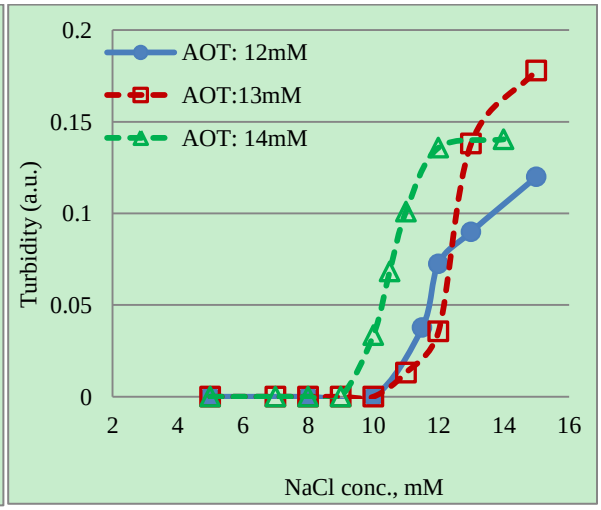

(d)

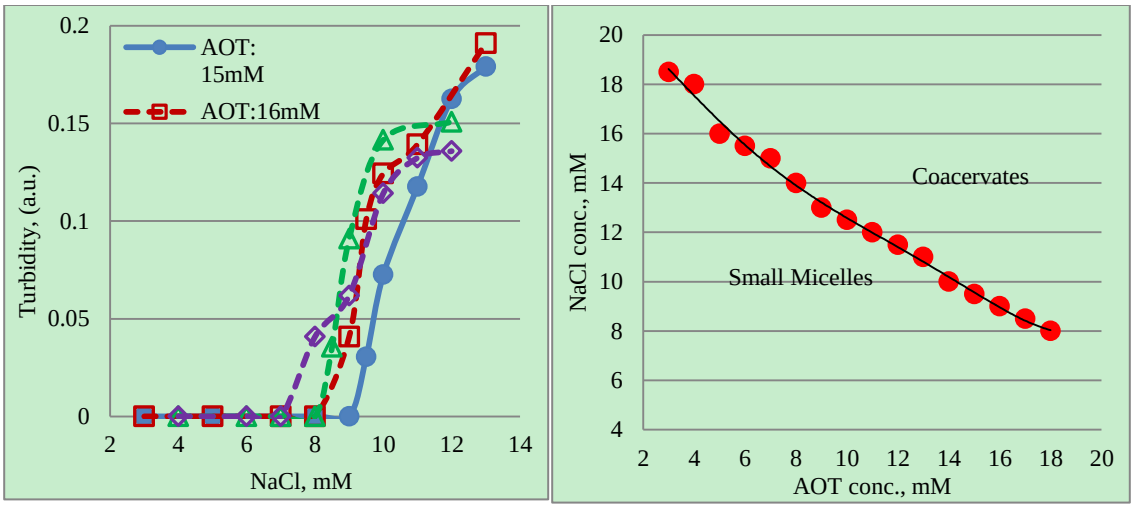

(e) (f)

Figure 3.1 Turbidity of the AOT/NaCl solutions with various AOT concentrations (a) AOT, 3mM, 4mM and 5mM, at different NaCl concentrations and 25 ℃. (b) AOT, 6mM, 7mM and 8mM at different NaCl concentrations and 25 ℃. (c) AOT, 9 mM, 10mM and 11mM at different NaCl concentrations and 25 ℃. (d) Turbidity of the AOT/NaCl solutions with fixed AOT concentrations of 12 mM, 13mM and 14mM at different NaCl concentrations and 25 ℃. (e) Turbidity of the AOT/NaCl solutions with fixed AOT concentrations of 15 mM, 16mM, 17mM and 18mM at different NaCl concentrations and 25 ℃. (f) AOT/NaCl coacervation phase boundary determination.

3.3.2 Counterion Binding degree

AOT has a special counterion binding behavior in aqueous electrolyte solution. Since counterions are known to influence CMC values of ionic surfactants, size and shape of ionic micelles and also reactions in solutions of ionic surfactants, investigating the counterion binding constant (β) of AOT/NaCl system is of fundamental importance. The counterion binding behavior of AOT/NaCl system has been conducted at 25 ℃ by Na^+ selective electrode measurement. The experimental procedure has been mentioned at experimental section. The values of β of AOT in aqueous NaCl media at 25°C were calculated using Corrin-Harkins (CH) equation (Corrin, et al. 1947).

$$\ln cmc = A - \beta \ln[C] \qquad (3.1)$$

In the above equation, [C] is the concentration of counterion in the solution and is taken as cmc+c_e and A is a constant related to the standard free energy of micellization. Since aggregation number increases with increased concentration of added electrolyte, β is varied with [C]. Umlong (Umlong, et al. 2005) and others reported that the β values of AOT in NaCl solution without coacervates. However, the β values of AOT in NaCl solution with coacervates has not been reported before. Thus, further study about β in coacervates solution is very important.

The sodium ion activity in the AOT solutions was directly determined from the EMF measurements using a sodium ion selective electrode. The measured electrode potential, E, is related to the activity of Na^+ by Nernst equation.

$$E = E_0 + S \log a_{Na} \qquad (3.2)$$

In equation (3.2), E_0 is a constant, reference potential and S is electrode slope. a_{Na} represents the level of sodium ions in solution. For AOT solution in water without the added electrolyte, the ion meter responses, E, is a function of AOT concentration. For determining the value of β of AOT in NaCl solution, an approach reported by Gaillon (Gaillon, et al. 1999) and Umlong (Umlong, et al. 2005) were employed. According to this method the experimental values of EMF for AOT in NaCl solution can be represented by the expressions

$$E = A_1 + B_1 \log(c_e + C_s) \qquad c_s<c_0 \qquad (3.3)$$

$$E = A_1 + B_1 \log[c_e + (1-\beta)c_s + \beta c_0] \qquad c_s>c_0 \qquad (3.4)$$

In equation (3.3) and (3.4), C_e is electrolytes concentration, C_s is AOT concentration and C_0 is cmc of AOT in electrolytes solution. A_1 and B_1 are the values of intercepts and slopes, respectively. They are obtained by least-squares fitting the E versus logC_t (C_t is

total free sodium ion concentration in solutions) data lying below the repective cmc values. The value of β of AOT in the presence of electrolytes obtained from the EMF data using equation (3.4). Two concentrations of NaCl were used to investigate. Their results are shown in Fig. 3.2 and Fig. 3.3, respectively. From two figures, it is obvious that the data fall on three different straight lines. The samples with AOT concentrations below the cmc were transparent solutions. In these samples, most of surfactants existed in solutions as free monomers and NaCl completely dissociated in solution as well. For the case of AOT concentrations below the cmc, β values for AOT are 0 because counterion binding does not occur in the solutions. Once the samples with AOT concentrations above the cmc, micelles were formed in the solution and Na^+ gradually attached to the surfactant headgroups. With more and more Na^+ bound on micelles, β value for AOT reached a constant. From equation (3.3) and (3.4), β was determined and shown in Table 3.1. With NaCl concentrations increasing, β value for AOT increases, which is in agreement with Umlong's (Umlong, et al. 2005) finding. The addition of NaCl into AOT aqueous solutions,

coacervates were formed in solutions and the solutions became cloudy. The reason is the structure of AOT micelles was changed. Wang (Wang, et al. 2014) and co-workers reported that AOT in aqueous solution self-assembles into vesicles and the vesicles changes into coacervates by introducing alkali metals. As seen in Fig. 3.2 and Fig. 3.3, the ion meter responses, E, for the samples of coacervates formed in AOT/NaCl/water system keep at a constant. This means the free Na^+ carried by coacervates has reached a maximum. β^* value for AOT coacervates samples are shown in Table 3.1. The change

of AOT micelles size in NaCl solutions can be further researched by DLS measurements.

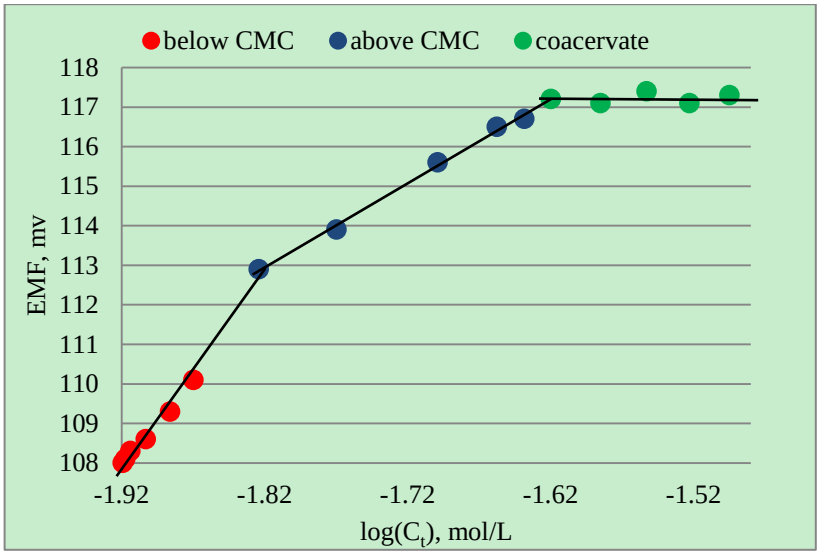

Figure 3.2 Ion meter response with the concentration of AOT in 12mM NaCl solution

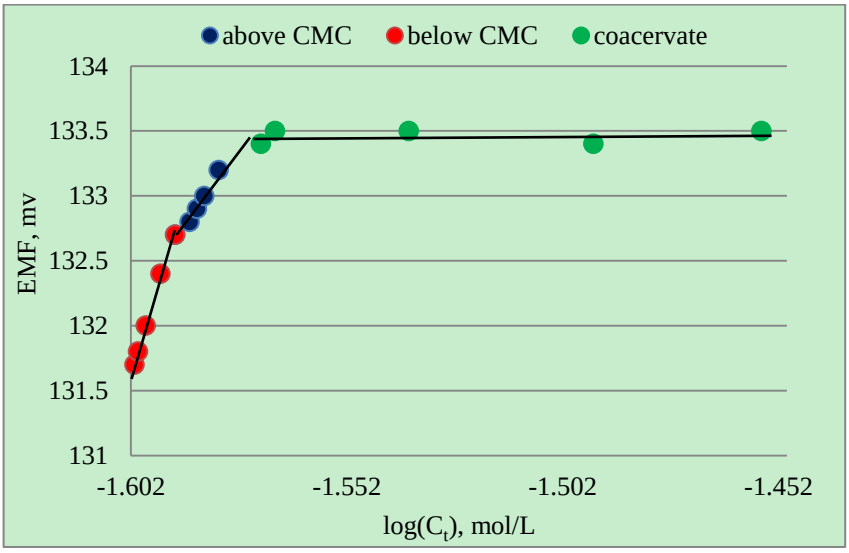

Figure 3.3 Ion meter response with the concentration of AOT in 25mM NaCl solution

Table 3.1 Values of cmc, β for AOT in NaCl solutions and β values in coacervates formed in solutions obtained from EMF measurements at 25 ℃

NaCl, mM	A_1, mV	B_1, mV	cmc, mM	β	β^*
12	187.04	41.18	1.49	0.37	0.62
25	303.65	107.38	0.62	0.65	0.91

*β values when coacervates formed

3.3.3 Size Distributions in Solutions

In order to measure the size of the aggregates of AOT in DI water and NaCl solutions, DLS measurements were carried out at three different cases and at same temperature. The first case (Fig.3.4(a)-(f)) was three different AOT concentrations (4, 10 and 20mM) in DI water solutions. The second case (Fig.3.5(a)-(j)) was 12mM AOT with five different NaCl concentrations (1.5, 5, 10, 11 and 14mM). The third case (Fig.3.6(a)-(l)) was the opposite of the second case. It fixed NaCl concentration at 25mM and varied AOT concentrations from 0.9mM to7mM. The size distribution profile was determined by NNLS (non-negative least squares) analysis. It is important to keep in mind that there is a very strong dependence of the intensity of light scattered, with respect to particle diameter. These two values have a sixth-power relationship. The number distribution shows the number of particles in different size bins. There is a first-power relationship between particle diameter and contribution to the distribution (Ranajay et al., 2011). The polydispersity index (PDI) is relatively low (~0.2).

In first case, Fig.3.4(a) shows the size distribution of 4mM AOT in DI water solution. There are two peaks in the figure. The small peak shows a diameter of about 16nm and the big peak shows a diameter of about 182nm. However, in the corresponding number distribution, there is only one peak at 16nm. AOT at 4mM is a slightly higher than the CMC of AOT in DI solution. Micelles are formed in the solution but the hydrodynamic

diameter is limited. The number distribution, Fig. 3.4(d), indicates that most of particles are existed as micelles in the solution. With the addition of AOT concentration up to 10mM, the particles grow constantly until 127nm, as seen in Fig. 3.4(b). In Fig. 3.4(b) and Fig. 3.4(e), the diameter of most of particles is about 127nm. Ranajay (Ranajay et al., 2011) and other researchers (Velázquez et al., 2007; Zhao et al., 2011) reported that relatively higher hydrodynamic diameter with size distribution indicates the formation of AOT vesicles rather than self-assembly of AOT molecules to form micelles. In Fig. 3.4(c), the first peak shows a diameter of about 100nm and the second peak shows a diameter of about 377nm. It is obvious that big aggregates take place at AOT 20mM. However, most of particles are existed as vesicles in the solution, as seen in Fig. 3.4(f). The three samples prepared for the first case are transparent and measured at 25 ℃.

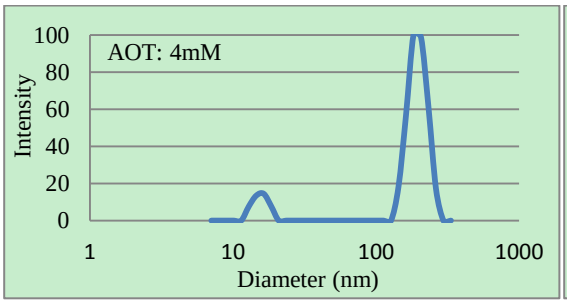

(a)

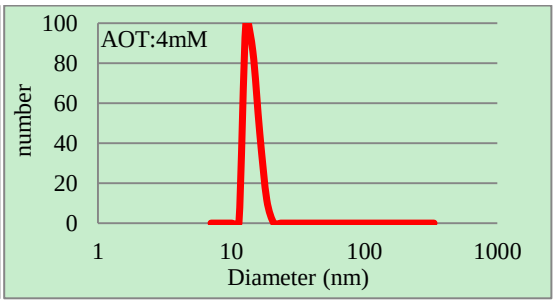

(d)

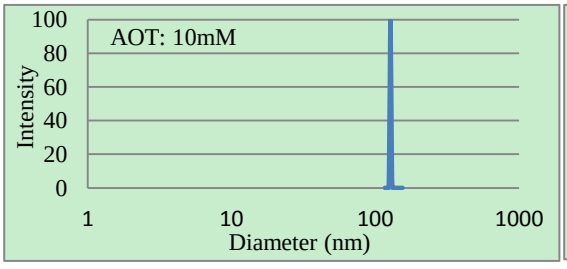

(b)

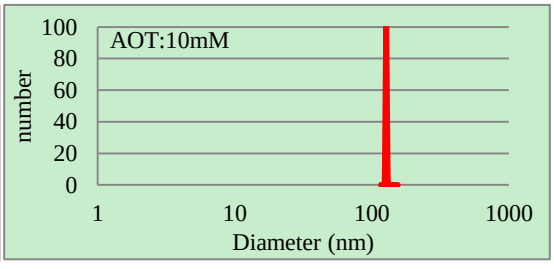

(e)

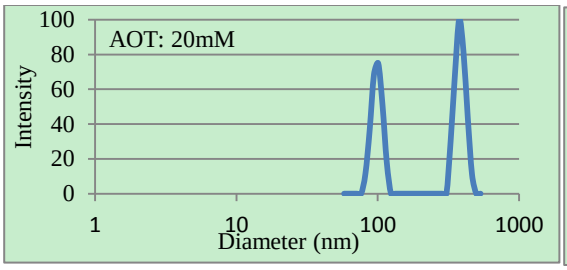

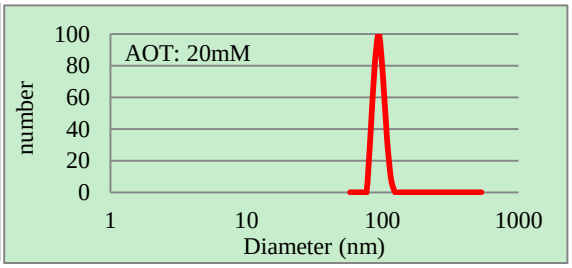

(c) (f)

Figure 3.4 (Left) Size distributions of the AOT/water aggregates at 25 ℃. (Right) Number distributions of the corresponding samples.

In second case (Fig.3.5 (a)-(j)), the similar evolution of particle size can be observed. From turbidity measurements, AOT concentration at 12mM, coacervates were formed at NaCl 11.5mM. In Fig.3.5 (d) and Fig.3.5 (i), since the concentrations of the sample is very close to the concentrations at boundary, big aggregates can be detected by DLS and showed on the number distribution. However, with the addition of NaCl concentration until 14mM, the peak denoted by big aggregates disappeared on the number distribution because the big aggregates settled on bottom of the vial and only supernatant was used to measure.

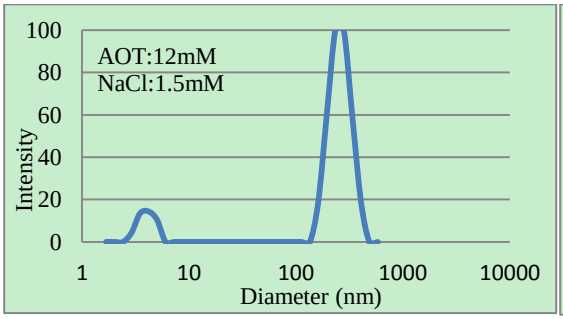

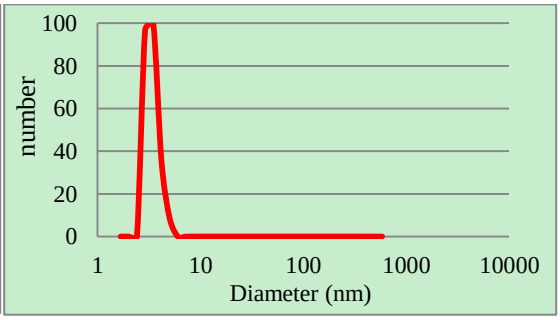

(a) (f)

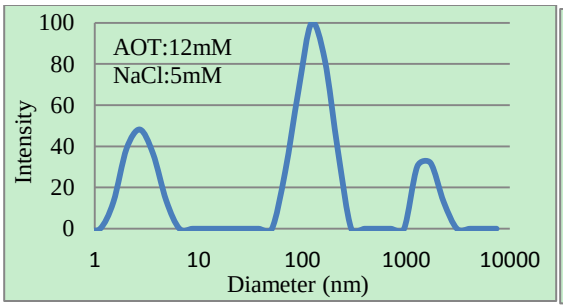
AOT:12mM
NaCl:5mM
Intensity
Diameter (nm)

(b)

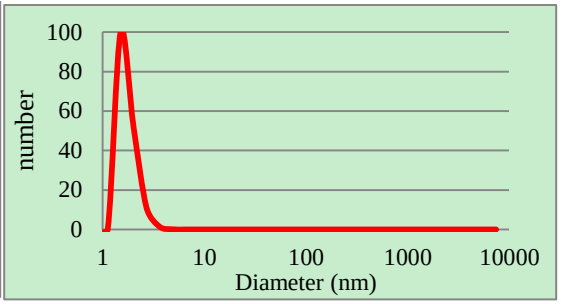
number
Diameter (nm)

(g)

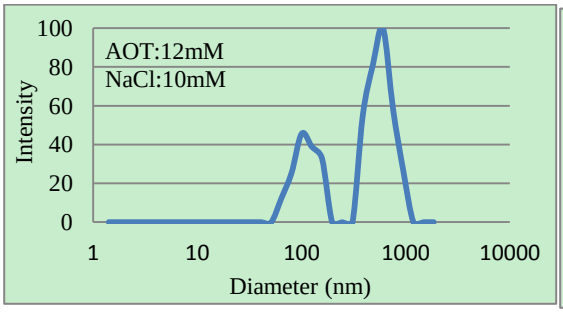
AOT:12mM
NaCl:10mM
Intensity
Diameter (nm)

(c)

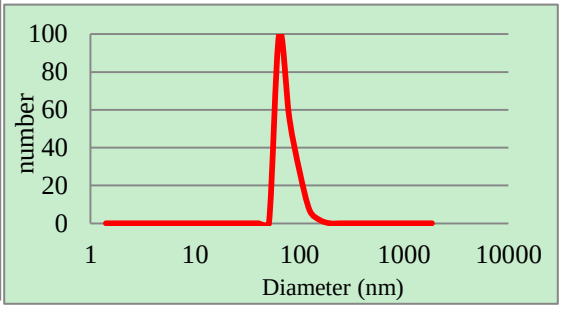
number
Diameter (nm)

(h)

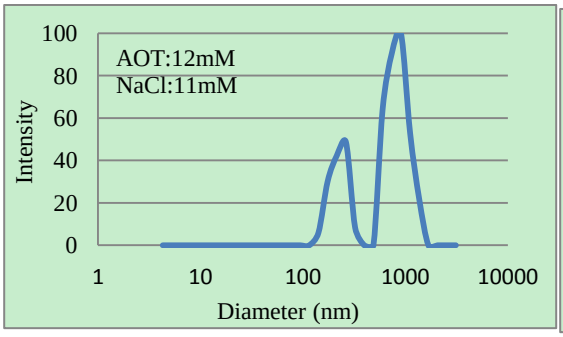
AOT:12mM
NaCl:11mM
Intensity
Diameter (nm)

(d)

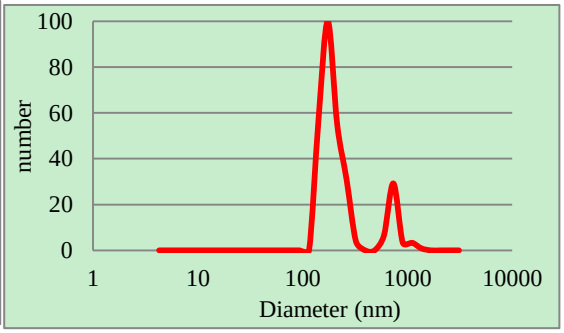
number
Diameter (nm)

(i)

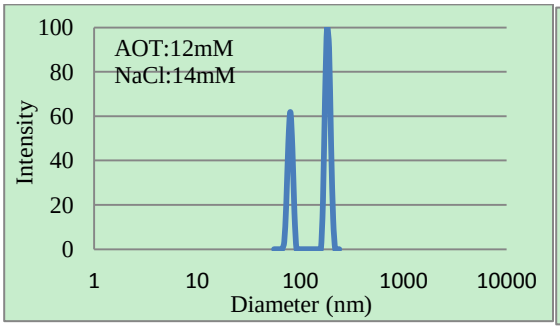
AOT:12mM
NaCl:14mM
Intensity
Diameter (nm)

(e)

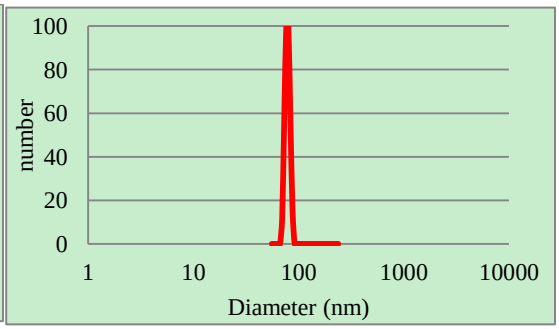
number
Diameter (nm)

(j)

Figure 3.5 (Left) Size distributions of the AOT at 12mM with different NaCl concentrations at 25℃. (Right) Number distributions of the corresponding samples.

In third case (Fig.3.6 (a)-(l)), NaCl concentration was fixed at 25mM and AOT concentrations varied from 0.9mM to 7mM. The results have the same trend as the above two cases. For NaCl at 25mM, the coacervates were formed at around 1.3mM. Therefore, the peak of big aggregates can be observed on Fig. 3.6(b), Fig. 3.6(c), and Fig. 3.6(d). And with AOT concentrations increasing, the peaks became narrow. The reason is the electrolytes in the solutions at a high level. For Fig. 3.6 (e) - (f), these two samples were very cloudy. After equilibrium, supernatant was used to measure and big aggregates settled on the bottom.

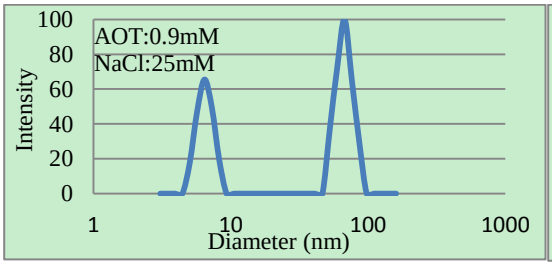

(a)

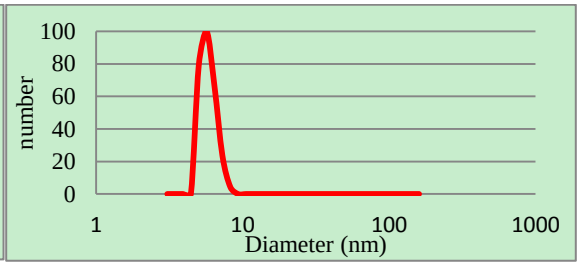

(g)

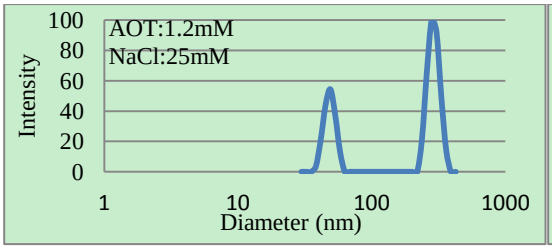

(b)

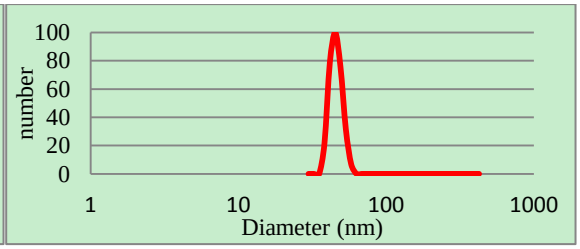

(h)

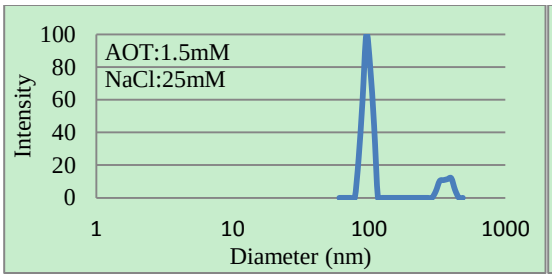

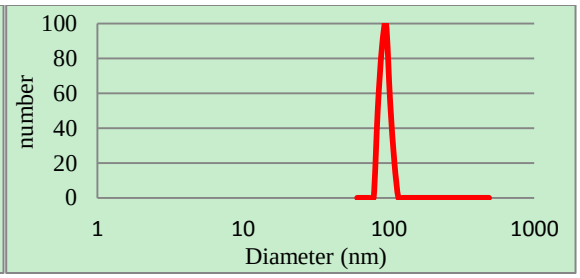

(c) (i)

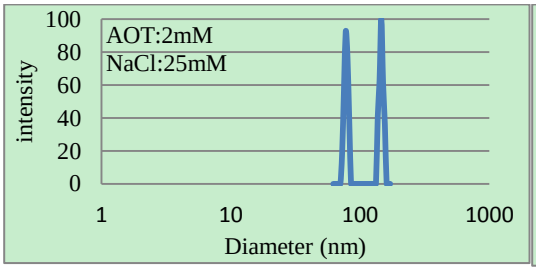

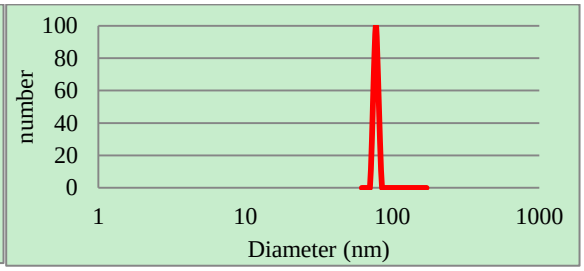

(d) (j)

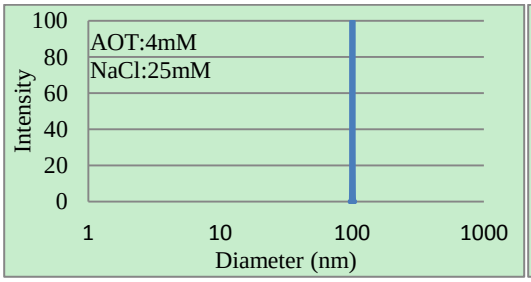

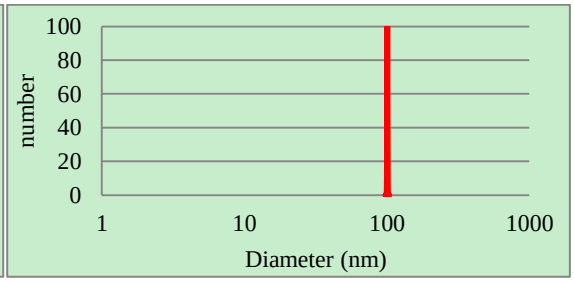

(e) (k)

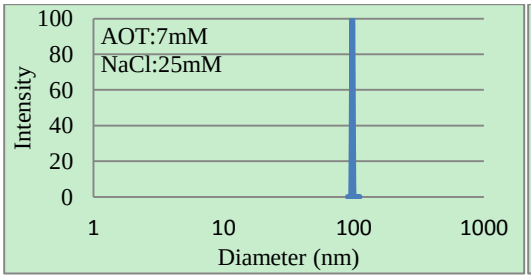

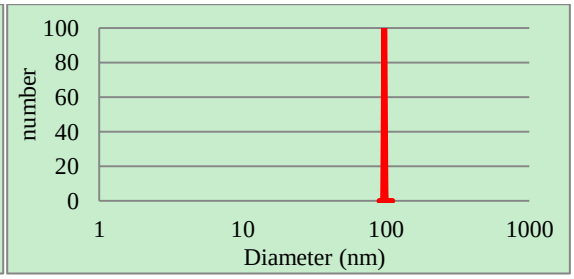

(f) (l)

Figure 3.6 (a) – (l). (Left) Size distributions of the different AOT concentrations at a constant NaCl concentration with 25mM at 25 ℃. (Right) Number distributions of the corresponding samples.

3.4 Conclusions

Coacervates boundary of AOT in the presence of NaCl clearly reveals an evolution in the particle size of AOT micelle. From the counterion binding constant, DLS results and literature reviews analysis the particle size change has been shown to be from micelles to vesicles and the vesicles change into the big aggregates. The value of β at coacervates in the solutions is higher than β of AOT for solutions below coacervates boundary. This is consistent with the finding made by Fujio (Fujio et al., 2005).

References

[1]. Menger, F. M. and Sykes, B. M. 1998. Anatomy of a coacervate. *Langmuir 14(1998): 4131-4137*

[2]. Wasilewski, T. 2010. Coacervates as a modern delivery system of hand dishwashing liquids. *J. Surfact Deterg 13(2010): 513-520*

[3]. Yeo, Y.; Bellas, E.; Firestone, W.; Langer, R.; Kohane, D. S. 2005. Complex coacervates for thermally sensitive controlled release of flavor compounds. *J. Agric. Food Chem. 53(2005): 7518-7525*

[4]. Saravanan, M. and Panduranga Rao, K. 2010. Pectin-gelatin and alginate-gelatin complex coacervation for controlled drug delivery: Influence of anionic polysaccharides and drugs being encapsulated on physicochemical properties of microcapsules. *Carbohydrate Polymers 80(2010): 808-816*

[5]. Feng, C.; Song, R.; Sun, G.; Kong, M.; Bao, Z.; Li, Y.;Cheng, X.; Cha, D.; Park, H.; Chen, X. 2014. Immobilization of coacervate microcapsules in multilayer sodium alginate beads for efficient oral anticancer drug delivery. *Biomacromolecules 15(2014): 95-996*

[6]. Goddard, E. D. 1990. Polymer/surfactant interaction. *J. Soc. Cosmet. Chem. 41(1990): 23-49*

[7]. Perry, L. S.; Li, Y.; Priftis, D.; Leon, L; Tirrell, M. 2014. The effect of salt on the complex coacervation of vinyl polyelectrolytes. *Polymers. 6(2014): 1756-1772*

[8]. Umlong, I. M. and Ismail, K. 2005. Micellization of AOT in aqueous sodium chloride, sodium acetate, sodium propionate, and sodium butyrate media: A case of two different concentration regions of counterion binding. *Journal of Colloid and Interface Science. 291 (2005): 529-536*

[9]. Kale, M. K.; Cussier, E. L.; Evans, D. F. 1980. Characterization of micellar solutions using surfactant ion electrodes. *J. Phys. Chem. 84 (1980): 593-598*

[10]. Wang, M.; Fan, Y; Nie, Z.; Wang, Y. 2013. Coacervation of cationic gemini surfactant with N-Benzoylglutamic acid in aqueous solution. *Langmuir 29 (2013): 14839-14847*

[11]. Kelley, G. E.; Murphy, R. P.; Seppala, J. E.; Smart, T. P.; Hann, S. D.; Sullivan, M. O.; Epps, T. H. 2014. Size evolution of highly amphiphilic macromolecular solution assemblies via a distinct bimodal pathway. *Nature Communications 5:3599 DOI: 10.1038/ncomms4599*

[12]. Corrin, M. L. and Harkins, W. D. 1947. The effect of salts on the critical concentration for the formation of micelles in colloidal electrolytes. *J. Am. Chem. Soc. 69 (1947): 683-688*

[13]. Chatterjee, A.; Moulik, S. P.; Sanyal, S. K.; Mishra, B. K.; Puri, P. M. 2001. Thermodynamics of Micelle formation of ionic surfactants: A critical assessment for sodium dodecyl sulfate, cetyl pyridinium chloride and dioctyl sulfosuccinate (Na Salt) by microcalorimetric, conductomietric, and tensiometric measurements. *J. Phys. Chem. B 105 (2001): 12823-12831*

[14]. Gaillon, L.; Lellèvre, J.; Gaboriaud, R. 1999. Counterion effects in aqueous solutions of cationic surfactants: Electromotive force measurements and thermodynamic model. *J. Colloid Interface Sci. 213 (1999): 287-297*

[15]. Wang, M. and Wang, Y. 2014. Development of surfactant coacervation in aqueous solution. *Soft Matter. 10 (2014): 7909-7919*

[16]. Saha, R.; Verma, P. K.; Mitra, R. K.; Pal, S. K. 2011. Structural and dynamical characterization of unilamellar AOT vesicles in aqueous solutions and their efficacy as potential drug delivery vehicle. *Colloids and Surfaces B: Biointerfaces 88 (2011): 345-353*

[17]. Velázquez, M.; Valero, M; Ortega, F.; González, J. B. R. 2007. Structure and size of spontaneously formed aggregates in Aerosol OT/PEG mixtures: effects of polymer size and composition. *Journal of Colloid and Interface Science 316 (2007): 762-770*

[18]. Zhao, K.; Jia, Z; Yang, L; Xiao, J. 2011. Dielectric spectra of Aerosol OT/Water systems at different concentrations and temperatures. *Chem. Res. Chinese Universities 2011, 27(6): 1065-1071*

[19]. Fujio, K.; Maruyama, Y.; Uzu, Y. 2005. Degree of counterion binding of Alkylpyridinium Halide Micelles: Its relation to micelle shape and size. *J. Oleo Sci. 54 (2005): 375-382*

[20]. Menger, F. M. and Peresypkin, A. V. 2001. A combinatorially-Derived structural phase diagram for 42 zwitterionic geminis. *J. Am. Chem. Soc. 123 (2001): 5614-5615*

[21]. Imura, T.; Yanagishita, H.; Kitamoto, D. 2004. Coacervate formation from natural glycolipid: One acetyl group on the headgroup triggers coacervate-to-vesicle transition. *J. Am. Chem. Soc. 126(2004): 10804-10805*

[22]. Xiao, Z.; Liu, W.; Zhu, G.; Zhou, R.; Niu, Y. 2014. A review of the preparation and application of flavor and essential oils microcapsules based on complex coacervation technology. *J. Sci. Food Agric. 94(2014): 1482-1494*

[23]. Puig, J. E.; Cota, L. Soltero-Martinez, J. F. A.; Gonzales-Romero, V. M.; Franses, E. I., "Effect of thermal and mixing history on the rheological properties of lyotropic liquid crystalline dispersions" in Mittal, K. L. and Shah, D. O., ed., *Surfactants in Solution, Volume 11,* Gainesville, Florida, 1991, pp. 207-217

Conclusions and Recommendations

Through systematic study for using ethyl formate shows it can be applied to SWCTT under high salinity conditions and mid-range temperature (<60 ℃). We believe that predicting the proper shut-in time beforehand could drastically reduce the risks of SWCTT operations in the field. For the foam study, stable dispersion by MWCNT is realized in developed foam formulations. The viscosity measurements show that the foam solution stabilized by MWCNT exhibits slightly high viscosity than the one without MWCNT. In addition, foam solution with MWCNT effectively generated in-situ foams in sand pack and propagated through sand pack. In coacervation study, the coacervate boundary coincides with increased sodium ion binding on surfactant aggregates. And DLS reveal increasing aggregate size approaching coacervate boundary. In addition, at coacervate boundary large aggregates with high counterion binding flocculate to form separate coacervate phase. Better understand coacervate is helpful to prepare formulations applied to EOR.

The most important recommendation for investigating foam is creating stable foam nanodispersion in the presence of oil. The pressure drop tests should be conducted in the presence of oil to see the impact of MWCNT for enhanced oil recovery, as well. The other important recommendation for studying coacervation is using Cryo-TEM to observe the structure of AOT aggregates.

Appendix A: Data Tables

Table A-1: Pressure drop (Formulation I) as a function of PV of liquid injected in foam flooding

PV	Pressure, psi	PV	Pressure, psi	PV	Pressure, psi	PV	Pressure, psi
3.00	0.96	3.62	4.55	4.17	12.13	4.76	14.87
3.06	0.92	3.64	4.58	4.19	12.27	4.78	14.87
3.07	0.94	3.65	4.67	4.20	12.34	4.79	14.87
3.09	0.94	3.67	4.77	4.21	12.41	4.81	14.89
3.10	0.97	3.68	4.94	4.23	12.69	4.82	14.92
3.12	1.01	3.70	5.04	4.25	12.88	4.84	14.93
3.13	1.04	3.71	5.15	4.28	12.96	4.85	14.93
3.15	1.06	3.73	5.38	4.29	13.04	4.87	15.01
3.16	1.13	3.74	5.62	4.30	13.12	4.88	15.04
3.18	1.23	3.75	5.77	4.32	13.13	4.90	15.05
3.19	1.33	3.77	6.23	4.33	13.18	4.91	15.17
3.21	1.45	3.79	6.59	4.35	13.22	4.93	15.19
3.22	1.58	3.80	6.86	4.36	13.33	4.94	15.23
3.24	1.65	3.81	7.13	4.38	13.36	4.96	15.31
3.25	1.76	3.83	7.4	4.39	13.42	4.97	15.35
3.26	1.8	3.84	7.63	4.41	13.47	4.99	15.35
3.28	1.96	3.86	7.84	4.42	13.48	5.00	15.35
3.30	2.07	3.87	8.21	4.44	13.53	4.76	14.87
3.31	2.14	3.89	8.68	4.45	13.62	4.78	14.87
3.33	2.24	3.90	8.89	4.47	13.68	4.79	14.87
3.34	2.43	3.92	9.06	4.48	13.76	4.81	14.89
3.36	2.56	3.93	9.28	4.50	13.89	4.82	14.92
3.37	2.78	3.95	9.47	4.51	13.91	4.84	14.93
3.39	2.89	3.96	9.72	4.53	14	4.85	14.93
3.40	2.96	3.98	9.93	4.54	14.16	4.87	15.01
3.41	3.03	3.99	10.32	4.56	14.24	4.88	15.04
3.44	3.64	4.00	10.51	4.57	14.26	4.90	15.05
3.46	3.76	4.01	10.65	4.59	14.41	4.91	15.17
3.47	3.91	4.03	10.83	4.60	14.46	4.93	15.19
3.49	3.99	4.04	10.89	4.61	14.47	4.94	15.23
3.50	4.01	4.05	10.99	4.63	14.49	4.96	15.31
3.51	4.11	4.07	11.15	4.64	14.56	4.97	15.35
3.52	4.14	4.08	11.28	4.67	14.59	4.99	15.35
3.53	4.19	4.10	11.38	4.69	14.64	5.00	15.35
3.55	4.31	4.11	11.5	4.70	14.72	-	-
3.56	4.36	4.13	11.67	4.72	14.73	-	-
3.59	4.44	4.14	11.84	4.73	14.74	-	-
3.61	4.49	4.16	11.98	4.75	14.83	-	-

Table A-2: Formulation I effluent in each sample (C_0=60mg/L)

PV	C/C_0
3.125	0
3.375	0
3.625	0.30
3.875	0.63
4.125	0.72
4.375	0.67
4.625	0.66
4.875	0.65
5.125	0.50
5.375	0.38
5.625	0.15
5.875	0.09
6.125	0.03
6.375	0
6.625	0
6.875	0
7.125	0
7.375	0
7.625	0
7.875	0

Table A-3: Pressure drop (Formulation II) as a function of PV of liquid injected in foam flooding

PV	Pressure, psi	PV	Pressure, psi	PV	Pressure, psi	PV	Pressure, psi
3	0.96	3.62	5.16	4.19	9.5	4.75	11.13
3.06	0.92	3.64	5.3	4.2	9.52	4.76	11.16
3.09	0.97	3.65	5.45	4.21	9.59	4.78	11.18
3.10	1.01	3.67	5.72	4.23	9.71	4.79	11.22
3.12	1.05	3.68	5.79	4.25	9.78	4.81	11.32
3.13	1.08	3.70	5.95	4.26	9.8	4.82	11.31
3.15	1.12	3.71	6.08	4.27	9.87	4.84	11.31
3.16	1.17	3.73	6.29	4.29	9.96	4.85	11.31
3.18	1.2	3.74	6.4	4.30	9.99	4.87	11.38
3.21	1.22	3.75	6.51	4.32	10.2	4.88	11.4
3.22	2	3.77	6.75	4.33	10.13	4.90	11.44
3.25	2.7	3.79	6.82	4.35	10.16	4.91	11.47
3.26	2.95	3.8	6.96	4.36	10.16	4.93	11.49
3.27	3.17	3.81	7.06	4.38	10.17	4.94	11.5
3.29	3.15	3.83	7.17	4.39	10.29	4.96	11.48
3.30	3.12	3.84	7.25	4.41	10.31	4.97	11.53
3.31	3.06	3.86	7.31	4.42	10.33	4.99	11.55
3.33	3.05	3.87	7.51	4.44	10.42	5	11.59
3.34	3.09	3.89	7.63	4.45	10.46	4.84	11.31
3.36	3.14	3.90	7.73	4.47	10.49	4.85	11.31
3.37	3.19	3.92	7.88	4.48	10.62	4.87	11.38
3.39	3.3	3.93	7.96	4.5	10.66	4.88	11.4
3.4	3.4	3.95	7.99	4.51	10.66	4.90	11.44
3.41	3.5	3.96	8.08	4.53	10.66	4.91	11.47
3.43	3.6	3.98	8.2	4.54	10.75	4.93	11.49
3.44	3.71	4	8.34	4.56	10.75	4.94	11.5
3.46	3.86	4.01	8.6	4.57	10.76	4.96	11.48
3.47	3.93	4.03	8.7	4.59	10.81	4.97	11.53
3.49	4	4.04	8.73	4.6	10.88	4.99	11.55
3.5	4.12	4.05	8.8	4.61	10.88	5	11.59
3.51	4.23	4.07	8.91	4.63	10.88	-	-
3.52	4.3	4.08	9.01	4.64	10.91	-	-
3.53	4.42	4.10	9.04	4.66	10.94	-	-
3.55	4.53	4.11	9.09	4.67	10.96	-	-
3.56	4.7	4.13	9.18	4.69	11.02	-	-
3.58	4.79	4.14	9.26	4.70	11.07	-	-
3.59	4.9	4.16	9.34	4.72	11.07	-	-
3.61	5.03	4.17	9.38	4.73	11.08	-	-

Table A-4: Formulation II effluent in each sample (C_0=58mg/L)

PV	C/C_0
3.125	0
3.375	0
3.625	0.32
3.875	0.66
4.125	0.74
4.375	0.81
4.625	0.91
4.875	0.94
5.125	0.86
5.375	0.72
5.625	0.62
5.875	0.5
6.125	0.34
6.375	0.15
6.625	0.04
6.875	0
7.125	0
7.375	0
7.625	0
7.875	0

Table A-5: Pressure drop (Formulation III) as a function of PV of liquid injected in foam flooding

PV	Pressure, psi	PV	Pressure, psi	PV	Pressure, psi	PV	Pressure, psi
3	0.94	3.62	6.64	4.16	15.53	4.70	18.37
3.09	2	3.64	6.6	4.17	15.71	4.72	18.39
3.10	2.27	3.65	6.6	4.19	15.92	4.73	18.41
3.13	2.86	3.67	6.6	4.2	16.1	4.75	18.43
3.15	3.28	3.68	6.59	4.21	16.29	4.76	18.43
3.16	3.52	3.70	6.59	4.23	16.42	4.78	18.43
3.18	3.67	3.71	6.9	4.25	16.56	4.79	18.45
3.19	3.77	3.73	7.03	4.26	16.65	4.81	18.48
3.21	3.97	3.74	7.03	4.27	16.76	4.82	18.49
3.22	4.17	3.75	7.05	4.29	16.83	4.84	18.5
3.24	4.37	3.77	7.06	4.30	16.87	4.85	18.5
3.25	4.54	3.79	7.05	4.32	16.88	4.87	18.51
3.27	4.79	3.8	7.05	4.33	16.88	4.88	18.52
3.28	5.09	3.81	7.22	4.35	16.91	4.90	18.53
3.30	5.27	3.83	7.47	4.36	16.9	4.91	18.56
3.31	5.45	3.84	7.7	4.38	16.88	4.93	18.58
3.33	5.57	3.86	7.89	4.39	16.87	4.94	18.6
3.34	5.7	3.87	8.21	4.41	16.89	4.96	18.61
3.36	5.84	3.89	8.65	4.42	16.99	4.97	18.61
3.37	6.01	3.90	9.08	4.44	17.15	4.99	18.6
3.39	6.09	3.92	9.55	4.45	17.29	5	18.61
3.4	6.29	3.93	9.82	4.47	17.37	-	-
3.41	6.43	3.95	10.26	4.48	17.49	-	-
3.43	6.55	3.96	10.65	4.5	17.56	-	-
3.44	6.67	3.98	11.01	4.51	17.62	-	-
3.46	6.72	3.99	11.42	4.53	17.67	-	-
3.47	6.78	4	11.62	4.54	17.76	-	-
3.49	6.9	4.01	11.95	4.56	17.82	-	-
3.5	6.93	4.03	12.42	4.57	17.88	-	-
3.51	7	4.04	12.83	4.59	17.93	-	-
3.52	7	4.05	13.12	4.6	18	-	-
3.53	7.05	4.07	13.55	4.61	18.06	-	-
3.55	7	4.08	13.98	4.63	18.11	-	-
3.56	6.97	4.10	14.38	4.64	18.17	-	-
3.58	6.9	4.11	14.72	4.66	18.21	-	-
3.59	6.8	4.13	14.99	4.67	18.27	-	-
3.61	6.6	4.14	15.26	4.69	18.32	-	-

Table A-6: Formulation III effluent in each sample (C_0=58mg/L)

PV	C/C_0
3.125	0
3.375	0
3.625	0.053621
3.875	0.37931
4.125	0.641379
4.375	0.724138
4.625	0.758621
4.875	0.775862
5.125	0.693103
5.375	0.62069
5.625	0.517241
5.875	0.431034
6.125	0.339655
6.375	0.15
6.625	0.036207
6.875	0
7.125	0
7.375	0
7.625	0
7.875	0

Table A-7: Pressure drop (Formulation III) as a function of PV of liquid injected in foam flooding (Liquid flow rate:0.3mL/min; Gas flow rate: 2.7mL/min)

PV	Pressure, psi	PV	Pressure, psi	PV	Pressure, psi	PV	Pressure, psi
3	0.91	3.67	2.1	4.12	4.13	4.59	6.27
3.21	0.91	3.69	2.1	4.13	4.14	4.6	5.95
3.22	1.11	3.70	2.1	4.15	4.15	4.61	5.67
3.25	1.34	3.72	2.11	4.16	4.21	4.63	5.61
3.26	1.4	3.73	2.18	4.18	4.31	4.64	5.6
3.27	1.45	3.72	2.11	4.19	4.59	4.66	5.6
3.29	1.57	3.73	2.18	4.21	4.65	4.67	5.6
3.30	1.66	3.75	2.25	4.22	4.83	4.69	5.6
3.32	1.8	3.76	2.33	4.25	5.07	4.70	5.57
3.33	1.9	3.78	2.37	4.26	5.07	4.72	5.5
3.35	2	3.79	2.41	4.27	4.96	4.73	5.45
3.36	2.06	3.81	2.48	4.29	4.91	4.75	5.42
3.38	2.07	3.82	2.54	4.30	4.88	4.76	5.41
3.39	2.09	3.84	2.65	4.32	4.88	4.78	5.41
3.41	2.11	3.85	2.69	4.33	4.88	4.79	5.41
3.42	2.14	3.87	2.77	4.35	4.89	4.81	5.48
3.44	2.15	3.88	2.88	4.36	4.96	4.82	5.63
3.45	2.15	3.90	3.04	4.38	5.11	4.84	5.74
3.47	2.15	3.91	3.17	4.39	5.26	4.85	5.77
3.48	2.15	3.93	3.33	4.41	5.33	4.87	5.64
3.5	2.15	3.94	3.39	4.42	5.31	4.88	5.54
3.51	2.15	3.96	3.39	4.44	5.1	4.90	5.53
3.53	2.15	3.97	3.39	4.45	5.13	4.91	5.52
3.54	2.15	3.99	3.41	4.47	5.13	4.93	5.52
3.56	2.15	4	3.49	4.48	5.17	4.94	5.58
3.57	2.14	4.01	3.6	4.5	5.25	4.96	5.72
3.59	2.14	4.03	3.73	4.51	5.43	4.97	26.8
3.6	2.13	4.04	3.87	4.53	5.65	4.99	6.06
3.63	2.12	4.06	3.97	4.54	5.84	5	6.1
3.64	2.12	4.07	4.05	4.56	6.06	-	-
3.66	2.12	4.09	4.09	4.57	6.21	-	-

Table A-8: Pressure drop (Formulation III) as a function of PV of liquid injected in foam flooding (Liquid flow rate:0.3mL/min; Gas flow rate: 20mL/min)

PV	Pressure, psi	PV	Pressure, psi	PV	Pressure, psi	PV	Pressure, psi
3	0.91	3.67	10.59	4.18	22.45	4.70	24.46
3.04	0.9	3.69	11.25	4.19	22.68	4.72	24.4
3.11	0.94	3.70	11.85	4.21	22.85	4.73	24.5
3.22	2.49	3.72	12.5	4.22	22.93	4.75	24.56
3.24	2.57	3.73	13.18	4.24	22.58	4.76	24.43
3.25	2.58	3.75	13.88	4.25	23.15	4.78	24.32
3.26	2.62	3.76	14.44	4.25	23.22	4.79	24.47
3.27	2.65	3.78	15.11	4.27	23.32	4.81	24.21
3.29	2.64	3.79	15.57	4.28	23.53	4.82	24.1
3.30	2.85	3.81	15.95	4.30	23.23	4.84	24.27
3.32	3.3	3.82	16.4	4.31	22.8	4.85	24.54
3.33	3.58	3.84	16.77	4.33	23.38	4.87	24.67
3.35	3.79	3.85	17	4.34	22.69	4.88	24.72
3.36	3.98	3.87	17.5	4.36	23.74	4.90	24.43
3.38	4.15	3.88	17.72	4.37	23.63	4.91	24.21
3.39	4.31	3.90	18.11	4.39	23.5	4.93	24.53
3.41	4.52	3.91	18.34	4.4	23.3	4.94	24.42
3.42	4.74	3.93	18.71	4.41	23.6	4.96	24.64
3.44	4.89	3.94	18.94	4.46	23.61	4.97	24.77
3.45	5.13	3.96	19.21	4.47	23.51	4.99	24.86
3.47	5.33	3.97	19.5	4.5	23.69	5	24.7
3.48	5.4	3.99	19.49	4.51	23.9	-	-
3.5	5.54	4	19.94	4.53	23.82	-	-
3.51	5.66	4.01	20.18	4.54	24.01	-	-
3.53	5.85	4.03	20.24	4.56	23.9	-	-
3.54	6.26	4.04	20.72	4.57	24.08	-	-
3.56	6.53	4.06	20.98	4.59	24.12	-	-
3.57	6.98	4.07	21.21	4.6	24.28	-	-
3.59	7.36	4.09	21.59	4.61	23.58	-	-
3.6	7.77	4.10	21.5	4.63	24.16	-	-
3.61	8.21	4.12	21.85	4.64	24.27	-	-
3.63	8.61	4.13	21.7	4.66	24.56	-	-
3.64	9.25	4.15	22.28	4.67	24.1	-	-
3.66	10	4.16	22.31	4.69	24.4	-	-

Table A-9: Degree of counterion binding with NaCl at 12 mM

AOT,mM	logCt , mol/L	EMF, mV	β
0.05	-1.91901	108	-
0.1	-1.91721	108.1	-
0.2	-1.91364	108.3	-
0.5	-1.90309	108.6	-
1	-1.88606	109.3	-
1.5	-1.86967	110.1	-
3	-1.82391	112.9	-
5	-1.76955	113.9	0.071
8	-1.69897	115.6	0.241
10	-1.65758	116.5	0.307
11	-1.63827	116.7	0.357
12	-1.61979	117.2	0.365
14	-1.58503	117.1	0.475
16	-1.55284	117.4	0.524
18	-1.52288	117.1	0.602
20	-1.49485	117.3	0.633

Table A-10: Degree of counterion binding with NaCl at 25 mM

AOT. mM	$\log C_t$, mol/L	EMF, mV	β
0.05	-1.601	131.7	-
0.1	-1.600	131.8	-
0.2	-1.599	132	-
0.4	-1.595	132.4	-
0.6	-1.592	132.7	-
0.8	-1.588	132.8	0.5
0.9	-1.587	132.9	0.52
1	-1.585	133	0.56
1.2	-1.582	133.2	0.58
1.8	-1.572	133.4	0.69
2	-1.569	133.5	0.69
4	-1.538	133.5	0.87
7	-1.495	133.4	0.94
10	-1.456	133.5	0.95